Hindawi Publishing Corporation
Journal of Medical Engineering
Volume 2014, Article ID 381251, 28 pages
http://dx.doi.org/10.1155/2014/381251

Review Article

Bioelectrical Impedance Methods for Noninvasive Health Monitoring: A Review

Tushar Kanti Bera

Department of Computational Science and Engineering, Yonsei University, Seoul 120749, Republic of Korea

Correspondence should be addressed to Tushar Kanti Bera; tkbera77@gmail.com

Received 31 August 2013; Revised 26 November 2013; Accepted 26 November 2013; Published 17 June 2014

Academic Editor: Norio Iriguchi

Under the alternating electrical excitation, biological tissues produce a complex electrical impedance which depends on tissue composition, structures, health status, and applied signal frequency, and hence the bioelectrical impedance methods can be utilized for noninvasive tissue characterization. As the impedance responses of these tissue parameters vary with frequencies of the applied signal, the impedance analysis conducted over a wide frequency band provides more information about the tissue interiors which help us to better understand the biological tissues anatomy, physiology, and pathology. Over past few decades, a number of impedance based noninvasive tissue characterization techniques such as bioelectrical impedance analysis (BIA), electrical impedance spectroscopy (EIS), electrical impedance plethysmography (IPG), impedance cardiography (ICG), and electrical impedance tomography (EIT) have been proposed and a lot of research works have been conducted on these methods for noninvasive tissue characterization and disease diagnosis. In this paper BIA, EIS, IPG, ICG, and EIT techniques and their applications in different fields have been reviewed and technical perspective of these impedance methods has been presented. The working principles, applications, merits, and demerits of these methods has been discussed in detail along with their other technical issues followed by present status and future trends.

1. Introduction

A living object such as an animal or plant is developed with cells and tissues arranged in three dimensional arrays. For example, the human body is a biological subject which is a very complex structure constructed by several living tissues [1] composed of the three-dimensional arrangement of human cells. The biological cells, containing intracellular fluids (ICF), cell membranes with or without cell wall, are suspended in the extracellular fluids (ECF) and show a frequency dependent behavior to an alternating electrical signal. Under an alternating electrical excitation, the biological cells and tissues produce a complex bioelectrical impedance or electrical bioimpedance [2–4] which depends on tissue composition and frequency of the applied ac signal [2–4]. Therefore the frequency response of the electrical impedance of the biological tissues is highly influenced by their physiological and physiochemical status and varies from subject to subject. Even the complex bioelectrical impedance varies from tissue to tissue in a particular subject and also varies with the change in its health status [5, 6] depending on the physiological and physiochemical changes occurred in the tissues health. Hence, the studies on complex bioimpedance of a tissue can provide a lot of information about its anatomy and physiology. Moreover, as the bioelectrical impedance of a body tissue depends on the signal frequency, the multifrequency studies on the electrical impedance of the biological tissues can potentially be used for the noninvasive investigations of their physiological or pathological properties.

Electrical impedance based noninvasive tissue characterizing techniques like bioelectrical impedance analysis (BIA) [7–21], electrical impedance spectroscopy (EIS) [22–32], electrical impedance plethysmography (IPG) [33, 34], impedance cardiography (ICG) [35–37], and electrical impedance tomography (EIT) [38, 39] are being used to study the frequency response of the electrical impedance of biological tissues. But EIS is found more popular in several fields of application compared to BIA, IPG and ICG as it

provides the impedance variations over frequencies. Also, EIS has been studied for the noninvasive characterization of biological as well as nonbiological materials in frequency domain whereas BIA, IPG and ICG are used in biological fields only. On the other hand, the BIA, IPG, and ICG are applied on biological tissues and, generally, at a particular frequency. BIA, IPG, and ICG all are impedance analyzing techniques which provide the impedance values of the tissue sample as a lumped estimation, whereas the bioelectrical EIS calculates and analyzes the electrical impedance at different frequencies which enable us to obtain not only the impedance values of the tissue sample as a lumped estimation at a suitable frequency (generally, 50 kHz) but also it provides the information to understand several complex bioelectrical phenomena like dielectric relaxation and dielectric dispersions. The information about the dielectric relaxation [40–42] and α, β, and γ dispersions [40–42] enables us to analyze and understand the complex bioelectrical phenomena [40–42] occurring in cells and tissues under an alternating electric current signal. BIA, EIS, IPG, and ICG investigate the tissue properties by assessing the lump impedance parameters obtained from the boundary voltage current measurement. On the other hand, EIT provides a spatial distribution (2D or 3D) of the impedance profile of a domain under test using a set of boundary voltage-current data. Therefore, EIT is found with the potential of visualizing the tissue physiology and pathology in terms of tomographic images of the electrical impedance distribution, and hence it has been applied in several applications.

The paper has discussed about the BIA, EIS, IPG, ICG, and EIT techniques and reviewed their technical perspective along with their application in different fields. The working principle, applications, merits, and demerits of all these methods have been discussed in detail in this paper along with their other technical issues. The paper discusses about the present status, challenges, and future directions of the impedance methods.

2. Bioelectrical Impedance

2.1. Biological Tissues and Their Bioelectrical Impedance. The animals or plants are the living subjects which are developed with cells and tissues arranged in three-dimensional (3D) space. Animals and plants are developed with animal tissues and plant tissues, respectively. The animal tissues and the plant tissues are composed of the 3D arrays of animal cells and plant cells, respectively. Human body is a complex biological structure composed of several tissues [1] composed of the 3D arrays of cells. All the biological cells, such as animal cells and plant cells, contain intracellular fluids (ICF) and cell envelop (cell membrane for animal cells and cell membrane and cell wall for plant cells) and are suspended in extracellular fluids (ECF). The animal cells and plant cells suspended in extracellular fluids (ECF) show a different behavior to an alternating electrical signal producing a complex electrical impedance [2–4] which is called bioelectrical impedance or electrical bioimpedance.

The bioelectrical impedance depends on the tissue composition as well as the frequency of the applied ac signal [2–4], and hence, the frequency response of the bioelectrical impedance of the biological tissues not only depends on their physiological and physiochemical status but also it varies with applied signal frequency. Moreover the bioelectrical impedance varies from tissue to tissue and subject to subject, even if it varies for the measurement directions in anisotropic tissue structures. Even the complex bioelectrical impedance changes due to the variation in tissue structure, composition, and health status [5, 6]. Hence, by studying the impedance analysis of biological tissue, one can obtain a lot of information about the tissue anatomy and tissue physiology. Therefore, the complex electrical impedance analysis of biological tissues is found to be an efficient tool for noninvasive investigations of physiological or pathological status.

2.2. Origin of the Bioelectrical Impedance. The biological subjects are developed with biological tissues which are developed with biological cells arranged in a very complex three-dimensional arrays suspended in extracellular matrix called an extracellular fluids (ECF) [5]. In animal tissue, the cells are composed of intracellular fluids (ICF), cell membranes (CM) which are suspended in extracellular fluids (ECF) whereas the plant cells are composed of ICF, CM, and cell wall (CW) and are suspended in ECF.

ICF, CM, and ECF all are composed of different materials having their distinguished electrical properties, and therefore each of these cell and tissue components respond distinguishably to an alternating current signal. The intracellular fluids are composed of the cytoplasm and the nucleus. The cytoplasm and the nucleus are mostly made up of solution of proteins, different chemicals, salts, and waters, and hence these materials are electrically conducting. The extracellular fluids are also made up of electrically conducting materials. As the intracellular fluids and extracellular fluids in biological tissues are composed of ionic solution and the highly conducting materials, they provide highly conducting paths (low resistive paths) to the applied current signal [34]. But, the cell membranes (Figure 1) of the cells in a biological tissue are composed of electrically nonconducting lipid bilayers (Figure 1(a)) sandwiched between two conducting protein layers [35, 36] and form the protein-lipid-protein (P-L-P) structures. In the P-L-P structures (Figure 1(b)) the hydrophobic tails do not absorb the water and hydrophilic heads are attached to the protein layers. The P-L-P [35, 36] sandwiched structure (Figure 1(c)) provides a capacitance [34] to the applied alternating current signal and contributes to a capacitive reactance.

As a result, the overall response of the biological tissues to an alternating electrical signal applied to it, produces a complex bioelectrical impedance (Z_b) [2–4] which is a function of tissue composition as well as the frequency of the applied ac signal [2–4]. The impedance Z_b is a complex quantity and varies with tissue structure, tissue composition, tissue health, and signal frequency. Therefore the impedance varies from subject to subject, tissue to tissue, and sometime with measurement direction within the same tissue. Even,

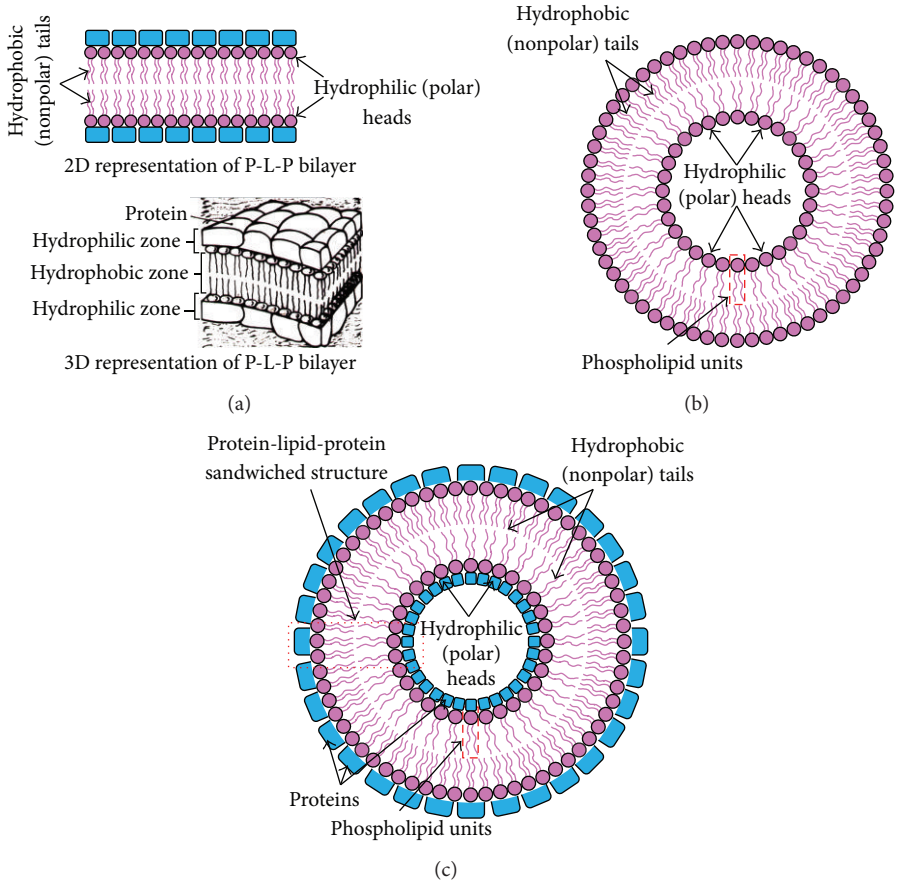

Figure 1: Cell membrane structure of the biological cells: (a) 2D and 3D model of P-L-P layers of a isolated cell membrane part, (b) 2D model of the lipid bilayers in cell membranes with hydrophilic (polar) heads and hydrophobic (nonpolar) tails, and (c) 2D model of the protein-lipid-protein sandwiched structure of a cell membrane.

the bioimpedance of a tissue may vary from other parts of the same tissue due to the variation in tissue composition, tissue physiology, and tissue pathology or tissue health.

2.3. Bioelectrical Impedance of Diseased Tissue. As the tissue physiology and pathology change with the tissue health, the bioelectrical impedance also varies from a healthy tissue to a diseased tissue. Thus the bioelectrical impedance changes with the variations in tissues health status [5, 6] such as swelling, disease, and infection. Similarly the impedance of a normal tissue is found more than a tumor or cancerous tissue as the cancerous tissue needs more blood to continue its rapid and uncontrolled growth which needs more blood. As the blood is good conductor of electricity, the cancerous tissue containing more blood shows a less impedance path to the electrical current.

2.4. Frequency Response of Bioelectrical Impedance. The frequency response of the bioelectrical impedance depends on their anatomical, physiological, and pathological status of the biological tissues. Therefore, the studies on the electrical bioimpedance of a tissue can provide a lot of information about its anatomy and physiology. As the response of the electrical bioimpedance varies with signal frequency, multifrequency impedance analysis provides more information about the tissue properties which help in the better tissue characterization. Therefore, the multifrequency impedance analysis of the biological tissues is found very promising for the noninvasive investigation of physiological or pathological status. As a result, a lot of research studies have been conducted on the single frequency impedance analysis as well as the multifrequency impedance analysis on biological tissues to investigate their physiological or pathological health status noninvasively for tissue characterization as well as for the diagnosis of a number of diseases.

3. Bioelectrical Impedance Analysis (BIA)

3.1. Impedance Measurement. Electrical impedance of a particular part of an object (volume conductor) is estimated by measuring the voltage signal developed across that body part by injecting a constant current signal to the object. Mathematically, the impedance (Z) is measured by dividing the voltage signal measured (V) by the current signal applied (I). Z is complex quantity and it will have a particular phase angle (θ) depending on the tissue properties. In electrical impedance measurement process, the bioelectrical

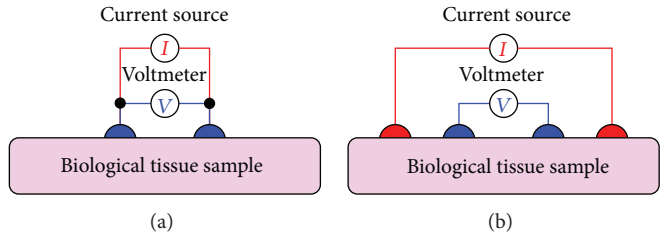

Figure 2: Bioelectrical impedance measurement in technique: (a) impedance measurement using two-electrode technique, (b) impedance measurement using four-electrode technique.

impedance of a body tissue is measured by injecting a low amplitude low frequency alternating current (generally sinusoidal) to the tissue through an array of surface electrodes attached to the tissue surface (tissue boundary). The alternating current is applied to avoid the tissue damage, and hence the bioimpedance measurement is never conducted with the direct current signal.

In BIA, the bioimpedance $Z\angle\theta$ is found as the transfer function of the SUT, and thus the $Z\angle\theta$ is calculated by dividing the voltage data ($V\angle\theta_1$) measured by applied current ($I\angle\theta_2$) as shown in

$$Z\angle(\theta) = \frac{V\angle(\theta_1)}{I\angle(\theta_2)}. \quad (1)$$

3.2. Two-Electrode and Four-Electrode Methods. The bioimpedance measurement process is conducted by either the two electrode or four-electrode methods. In both the methods, the surface electrodes through which the current signal is injected are known as the current electrodes or the driving electrodes (as shown by the red colored electrodes in Figure 2) and the electrodes on which the frequency dependent ac potential ($V(f)$) is measured are called voltage electrodes or sensing electrodes (as shown by blue colored electrodes in Figure 2).

As the name tells, the two-electrode method (Figure 2(a)) uses only two electrodes for impedance measurement, and hence the current signal injection and voltage measurement are conducted with same electrodes. The two-electrode-method, therefore, suffers from the contact impedance problem and the measurement data contains the voltage drop due to the contact impedance. In the four-electrode method (Figure 2(b)), two separate electrode pairs are used for current injection and voltage measurements, and hence the four-electrode method is found as an impedance measurement method with a linear array of four electrodes attached to the SUT as shown in Figure 2(b). The four-electrode method injects a constant amplitude current signal to the SUT through the outer electrodes called current electrodes or the driving electrodes (red colored electrodes in Figure 2(b)) and the frequency dependent developed voltage signals are measured across two points within the current electrode through the inner electrodes called voltage electrodes or the sensing electrodes (blue colored electrodes in Figure 2(b)).

3.3. Bioelectrical Impedance Analysis. Bioelectrical impedance analysis (BIA) is a technique in which the body composition of a biological object is analyzed by measuring its bioelectrical impedance. Hence the bioelectrical impedance analysis measures the bioimpedance of the tissue which is produced inside the biological object when an alternating current tends to flow through it, and hence it is found as a function of tissue properties as well as the applied current signal frequency. As explained earlier, like other electrical impedance measurement techniques, in bioimpedance measurement methods, a constant sinusoidal current is injected to the subject under test (SUT), or a biological tissue sample, and the voltage developed is measured using four-electrode method [5] or four-probe method, and the electrical impedance of the SUT is calculated. In four-electrode method of bioimpedance measurement process, a constant amplitude alternating current is injected through two electrodes (outer electrodes) called current electrodes and the voltages are measured on other two electrodes (inner electrodes) named as voltage electrodes as shown in Figure 2 [5]. BIA determines the bioelectrical impedance of a particular body part attached with surface electrodes [5]. Bioelectrical impedance of a subject can be used to calculate an estimate of the body composition.

A bioelectrical impedance analysis (BIA) [7–14] is a technique in which the body composition [14–21] of a biological object is analyzed by measuring its electrical impedance called bioelectrical impedance or electrical bioimpedance. Dr. William Mills, M.D., an Admiral in the US Navy, initiated the study on BIA in Mount McKinley, Alaska, in 1981, to assess the hydration status of soldiers in high altitude cold weather environments. The paper published by Hoffer et al. [7] in 1969 indicated a procedure to predict the total body water by measuring the hand to foot whole body BIA and with the encouragement of Jan Nyboer the Mount McKinley soldier hydration project was started. Shortly thereafter Lukaski et al. [8] at the USDA in Grand Forks, ND, published the first to a paper on BIA and body composition.

3.4. Body Compositions. Human body is developed with the complex arrangement of different body tissues consists of water, protein, fat, and minerals called the body compositions. The human body is composed of 64% water, 20% protein, 10% fat, 1% carbohydrate, and 5% minerals approximately [15] as shown in Figure 3(a). Over 90% of

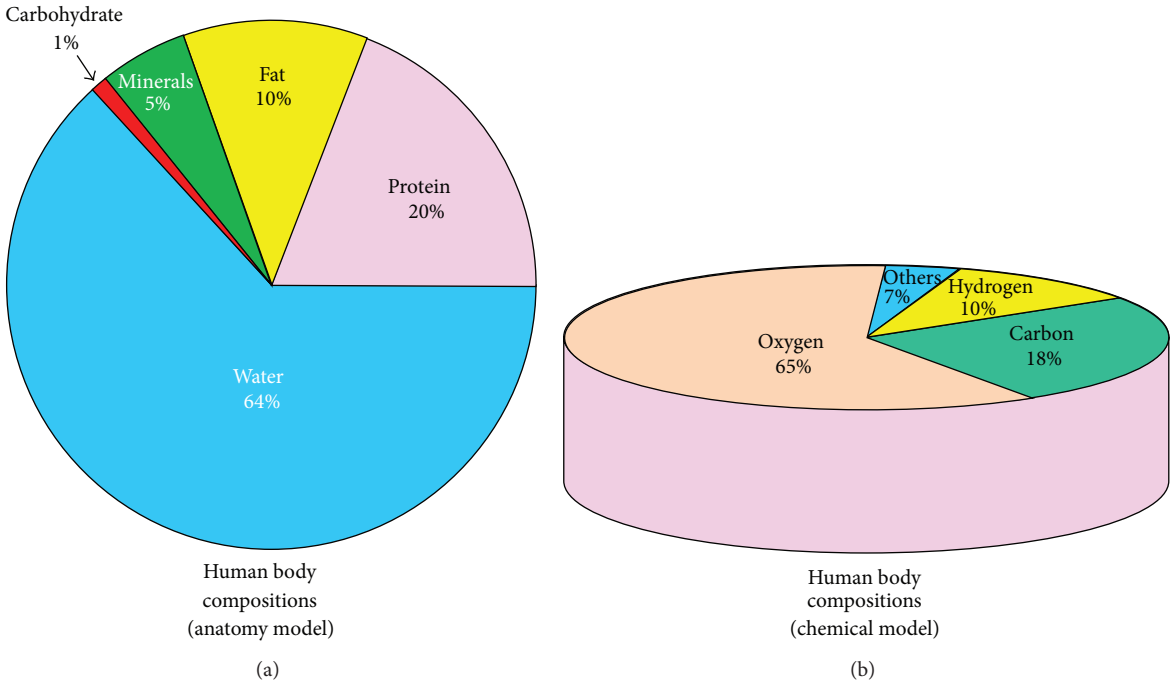

Figure 3: Compositions of human body: (a) anatomy model of the human body composition percentage of fat, protein, minerals, and liquid in an adult human subject; (b) chemical model of the human body composition percentage of different elements in the body composition of human subjects.

the mass of the human body is made by the just three elements, namely, oxygen (65%), carbon (18%), and hydrogen (10%) among 118 elements discovered so far (Figure 3(b)). The human body compositions are largely divided into two groups: body fat and lean body. The lean body is divided to protein, mineral, and body water. Protein is a main element of muscles, whereas the minerals are found mostly in bones [43]. Total body water (TBW) consists of intracellular water (ICW) and extracellular water (ECW). ICW are found within the cells and tissues and give cell volume and tissue volumes whereas the ECW is composed of blood, lymph, and so forth [43]. Body cell mass is the sum of ICW and metabolically active tissues [43]. The body-composing constituents and their explanation and function are presented in Table 1. Body composition (Figure 3(a)) of human subject is essentially to be estimated to study and diagnose the normal health, diseases, and the other abnormal health status. Human body mass is developed with several elements (Figure 3(b)) in form of water, cells, and tissues. Human body mass consists of tissues with high conductivity called lean body mass (LBM) and tissues with low conductivity called body fat (BF). Generally, an unhealthy body composition refers to carrying too much fat in comparison to lean tissue (muscle), and the more the body's fat, the more the health risks. In fact, unhealthy body composition often leads to obesity creating many other health complications like heart disease, stroke, high blood pressure, high cholesterol, type 2 diabetes, back pain, and so forth.

Table 1: Body-composing constituents and their explanation and function [43].

Body-composing constituents	Explanation and function
Intracellular water (ICW)	Body water which exists inside of cell membrane
Extracellular water (ECW)	Body water that exists outside of cell membrane (blood, interstitial fluid, etc.)
Body water	The sum of intracellular and extracellular water
Protein	Main element which composes soft lean mass together with water
Soft lean mass (SLM)	Skeletal muscle and smooth muscle Maintaining body function
Minerals	Composing bones and electrolytes
Lean body mass (LBM)	Composed with soft lean mass and minerals The amount of body weight minus body fat mass
Body fat	The amount of body weight minus lean body mass
Weight	The sum of lean body mass and body fat mass. Standard weight (kg): adult male height (m) × height (m) × 22 female height (m) × height (m) × 22

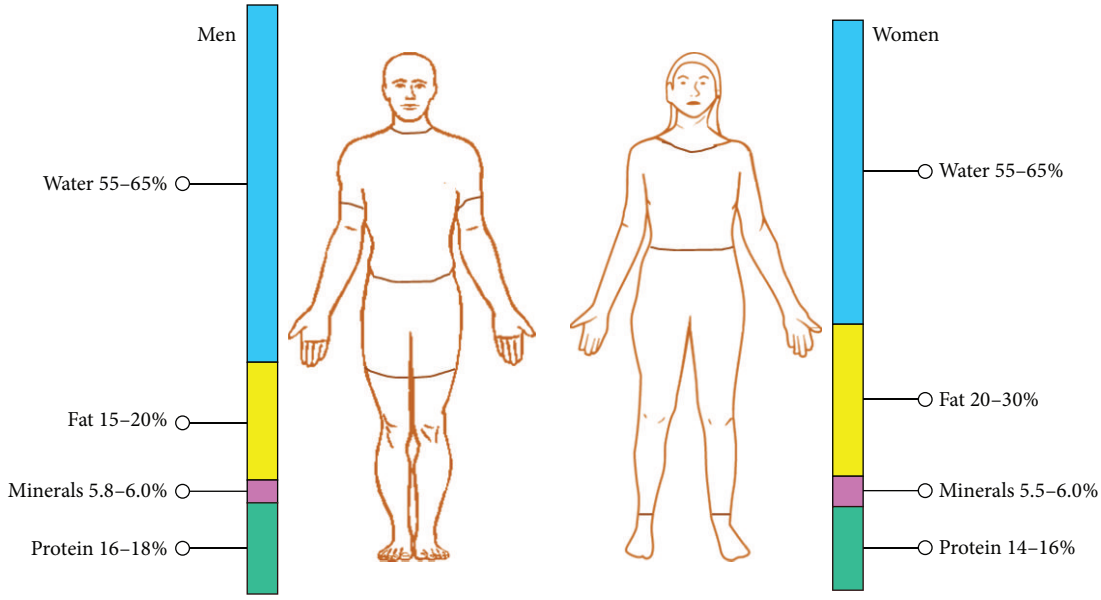

Figure 4: Optimal ratio of body composition.

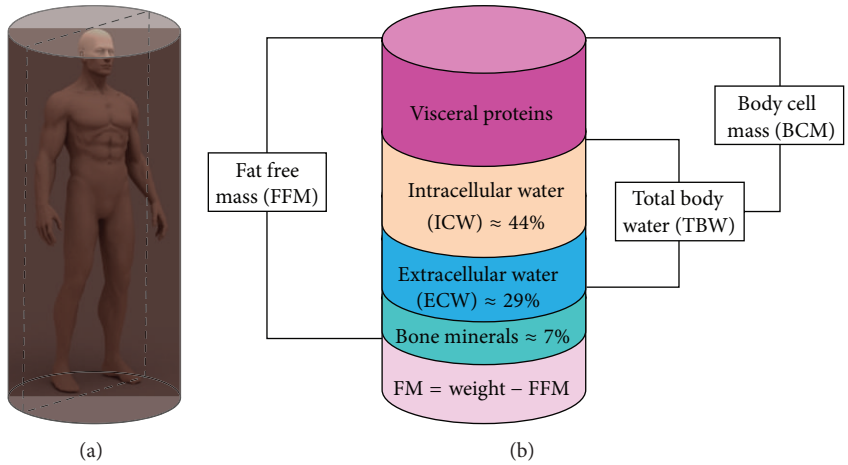

Figure 5: Human body as a conducting cylinder and its body composition: (a) human body assumed as a conducting cylinder in BIA, (b) body composition schematic diagram of fat-free mass (FFM), total body water (TBW), intracellular water (ICW), extracellular water (ECW), and body cell mass (BCM) [9].

3.5. Optimal Ratio of Body Composition for Male and Female. The optimal ratio of body composition is shown in Figure 4. In human body the following relations are held for body compositions:

(1) lean body mass ∝ soft lean mass ∝ body water;

(2) lean body mass ∝ 1/percent of body fat;

(3) lean body mass varies directly as soft lean mass or body water but inversely as body fat mass;

(4) because of weight = lean body mass + body fat.

3.6. BIA and Body Composition Calculation

3.6.1. Fat-Free Mass (FFM) or Lean Body Mass (LBM). The fat free mass (FFM) or the lean body mass (LBM) or muscle mass or body cell mass (BCM) [9] is developed with muscle as well as the metabolically active tissue in your organs [9]. Fat-free mass is comprised of the nonfat components of the human body. Skeletal muscle, bone, and water are all examples of fat-free mass. Several equations are proposed to calculate the fat-free mass. The schematic diagram of the body composition such as fat-free mass (FFM), total body water (TBW), intracellular water (ICW), extracellular water (ECW), and body cell mass (BCM) is shown in the Figure 5.

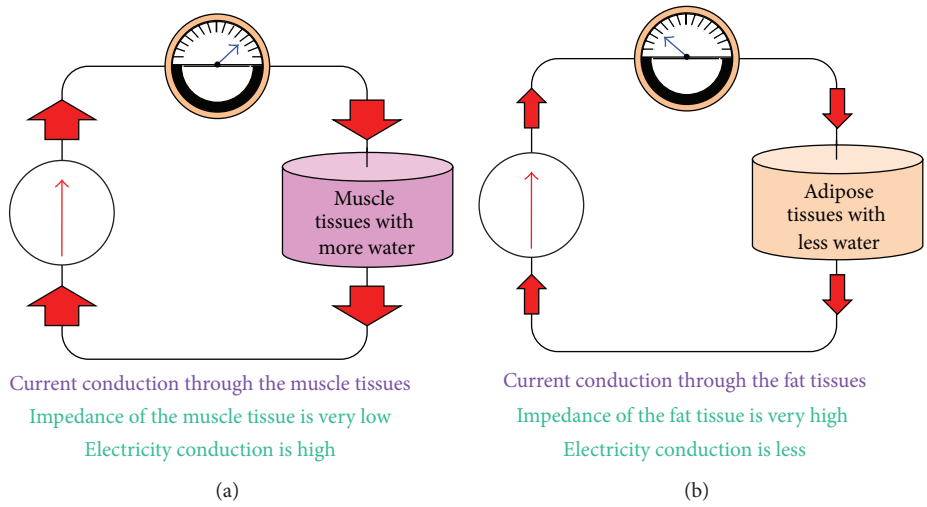

FIGURE 6: Current conduction through body tissues (a) through muscle tissue and (b) through fat tissue.

The following equations have low standard errors for predicting FFM and is appropriate for the general population [44]:

for females:

$$\text{Fat-Free Mass (kg)} = 0.475 \times \left[\frac{(\text{ht (cm)})^2}{R\,(\text{ohms})}\right] + 0.295 \times \text{wt (kg)} + 5.49; \quad (2)$$

for males:

$$\text{Fat-Free Mass (kg)} = 0.485 \times \left[\frac{(\text{ht (cm)})^2}{R\,(\text{ohms})}\right] + 0.338 \times \text{wt (kg)} + 3.52. \quad (3)$$

3.6.2. Body Fat (BF). The body fat is the amount of fat tissue within a body that is the total adipose tissues without any muscle tissue or body fluids or electrolyte [9]. It is the total body mass minus the FFM:

$$\text{Body Fat (BF) (kg)} = \text{Total Body Mass (TBM) (kg)} - \text{Fat-Free Mass (kg)}. \quad (4)$$

3.6.3. Total Body Water Body (TBW). Several formula of total body water body (TBW) has been proposed by different research groups. Body water consists of intracellular water (ICW) and extracellular water (ECW) [18]. Total body water body (TBW) is given by [18]:

$$\text{TBW (kg)} = 1.84 + 0.45\left(\frac{\text{height}^2\ \text{square}}{\text{resistance}}\right) + 0.11\,(\text{weight}). \quad (5a)$$

According to Lukaski et al. [8] and the Jawon Medical Inc. [43], South Korea, the formula is given by:

$$\text{TBW (kg)} = 0.377\left(\frac{\text{height}^2}{\text{resistance}}\right) + 0.14\text{Weight} - 0.08\text{Age} + 2.9\text{Gender} + 4.65, \quad (5b)$$

$$\text{TBW (kg)} = \text{A} \times \left(\frac{\text{height}^2}{\text{resistance}}\right) + \text{B} \times \text{Weight} - \text{C} \times \text{Age} + \text{D} \times \text{Gender}, \quad (5c)$$

where A, B, C, D, and E are the constants.

3.7. Body Tissue Conductivity. Fat tissues are the adipose tissues consisting of fat cells, which are a unique type of cell containing electrically low conductive materials. The fat tissue impedance is high as the conductivity of the fat tissue is low (Figure 6(a)). On the contrary, lean tissues contain intracellular and extracellular fluid and electrolytes. Therefore, as the conductivity of the lean tissue is high, the impedance is low in lean tissues (Figure 6(b)). Impedance is thus proportional to TBW. Under an alternating current inject to the body, the current signal flows along with paths contain more water within the body since it has high conductivity. Depending on the water content in the body, the impedance value changes for body water, body fat, and body muscle. The ratio of these two types of tissues is reflected on the electrical characteristic and the impedance value [45].

3.8. BIA for Body Composition and Health: The Necessity. In a healthy human body, a certain ratio of the compositions is maintained to sustain a good health. Hence, the body composition assessment is essential to study the human health as well as to diagnose a number of diseases like obesity, edema, and protein-deficient malnutrition as well as to assess the metabolic status in human body. Though there are several methods to assess the body compositions like skin-fold test

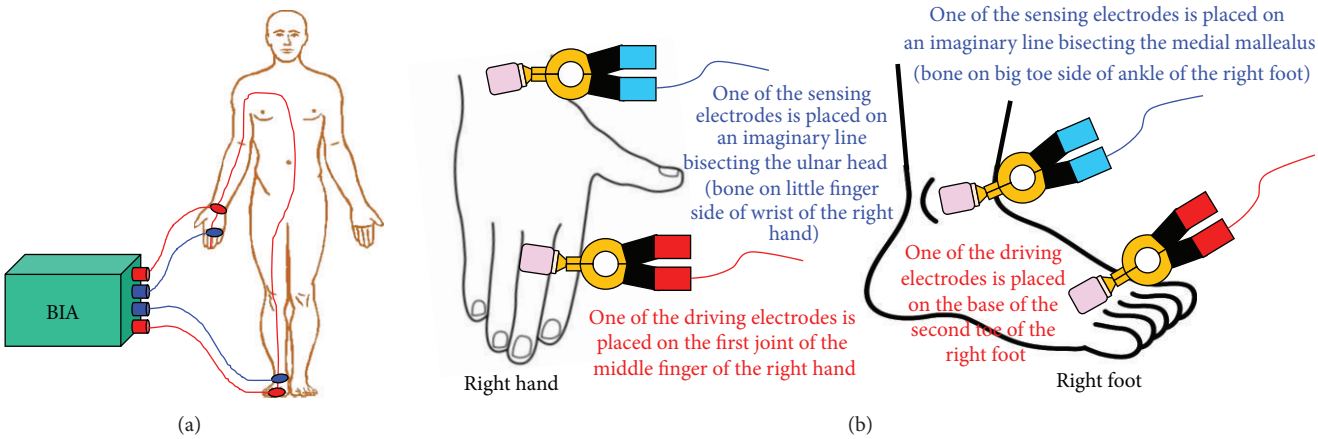

Figure 7: Body composition assessment using BIA: (a) BIA current injection and voltage measurement schematic; (b) electrode connection in impedance measurement procedure of the BIA.

[21, 45], underwater weighing [21, 45], waist-to-hip ratio method [46], and dual energy X-ray absorptiometry (DEXA) [47]; still the accurate, noninvasive, low cost, fast and easy methods are always desired in medical and clinical fields for body composition assessments. In this direction, bioelectrical impedance analysis (BIA) which is able to properly identify a subject's health risk of excessively high or low body fatness is being studied and researched by a number of research groups including doctors, clinicians, medical practitioners, and biomedical engineers. It is a growing and promising technique that ranks similar to skin-fold measurement in its accuracy, precision, and objectivity [48]. BIA is used to study, analyze, and evaluate the body fat and body fat free mass. BIA also shows many other health parameters such as your BMI (body mass index) and total body water (TBW).

3.9. Advantages of BIA. Compared to the other noninvasive procedures to assess the body compositions, the BIA technique has the following advantages:

(i) noninvasive, safe, fast, low cost, portable, easy to conduct, hazards free, and safe technique;

(ii) measures fat-free mass and calculates fat mass;

(iii) calculates of body cell mass, total body water, intracellular water, and extracellular water;

(iv) BIA devices are light in weight, portable and can be used at the bedside;

(v) BIA devices can be used to assess total body water in individuals with altered metabolic function;

(vi) excellent consistency for repeated measurements.

3.10. BIA Procedures. BIA is studied with an instrument, called body composition analyzer (BCA) (Figure 7(a)), which is dedicated to inject a constant current and measure the electrical impedance of the body (Z_B) using standard four-electrode method (Figure 7(b)). As explained earlier, in four-electrode method based BIA procedure, a low and constant amplitude (≤1 mA) alternating current (generally 50 kHz) is injected through two electrodes (outer electrodes) called current electrodes and the voltages are measured on other two electrodes (inner electrodes) named as voltage electrodes as shown in Figure 7(b). The resistance (R) or resistivity (ρ) is calculated from the impedance (Z_B), and using the resistivity or conductivity, various body compositions are calculated as shown in Section 3.6.

3.11. Assumptions in BIA Calculations. The BIA assumes the human body as a cylindrical homogenous conductor (Figure 8)whose impedance is proportional to the length and inversely proportional to the cross-sectional area of the base (Figure 8).

Though, in practical case, the human body is different from the assumptions mentioned above, but for ease of calculation, the BIA formulation procedures, generally, have the following assumptions:

(1) human body is a cylinder determined by height and weight;

(2) body composition is homogenous and evenly distributed;

(3) there are no individual differences and variations within the body compositions;

(4) there are no changes in the environment (temperature), body heat, and stress.

The BIA procedure applies an alternating current which experiences a bioelectrical impedance exerted by the cells and extracellular fluids. As the cell membranes are capacitive in nature, the capacitive reactance produced by the electric current applied selectively allows the current pass through it depending on the signal frequency and hence the current paths (Figure 8). The low frequency current passes through the extracellular fluids as the cell membrane reactance does not allow the low frequency current to pass through it whereas the high frequency current penetrates the cell membranes and passes through both the extracellular fluids and the cells (membranes and intracellular fluids). Thus by

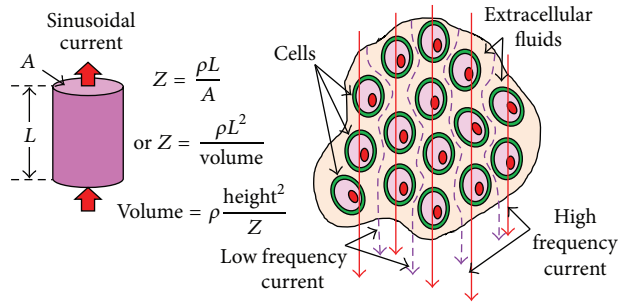

FIGURE 8: Impedance of the human body assuming it as a homogeneous cylindrical volume conductor.

applying the alternating current at a particular frequency, BIA procedure can assess the amount of extracellular water (ECW), intracellular water (ICW), and total body water (TBW = ECW + ICW).

3.12. BIA Outcomes. The BIA results reveal several information about the body composition and the body health such as

(i) LBM and BF ratio: how much lean body mass (LBM) versus body fat (BF) a person has;

(ii) Toxic burden: how much the toxic burden of the human subject is;

(iii) Water intake: whether the person is drinking adequate amount of water or not;

(iv) Burning calories: how many calories the person is burning at rest;

(v) Loosing and gaining of LBM or BF: whether the subject is losing or gaining muscle mass or fat;

(vi) Health status: how healthy the person's cells are.

3.13. BIA Preparations and Precautions. The BIA procedure is conducted on the patients by attaching few electrodes on their body and the entire experimentation is completed within 3-4 minutes. The BIA experimentation is conducted on the patients, either in lying or standing condition, with the electrodes attached to the body, and a small amount of alternation current is injected, and the potentials are measured. The amplitude of the electrical current is so small that it cannot be felt at all. The BIA procedures are conducted on the subject who should not

(1) eat or drink caffeine for 4 hours prior to your appointment,

(2) exercise for 12 hours prior to the person's appointment,

(3) wear tight clothing or pantyhose,

(4) apply lotion on the person's hands and feet prior to your appointment and

(5) let the person take his diuretic medication within 6 hours prior to your appointment.

The BIA procedures are conducted on the subject who should

(1) remove all metal jewellery prior to doing the assessment and

(2) drink 2–4 glasses of water within 2 hours of your appointment.

3.14. BIA Procedure Cost. Bioelectrical impedance analysis (BIA) is a simple, safe, noninvasive, and painless procedure which is conducted by a single person: a doctor, medical practitioner, clinician, nurse, or even a laboratory expert. The approximate cost of a BIA experiment is around \$35–\$65 [49]. The BIA test fee in Healthy Directions, Nutrition Therapy, and Counseling Center of Doylestown Hospital, USA, is \$25 [50].

3.15. Single Frequency BIA and Dual Frequency BIA. Researches show that the alternating current BIA can be performed in either single frequency current (called single frequency BIA or SFBIA) or dual frequency current (called dual frequency BIA or DFBIA) [51]. Generally, SFBIA is performed with 50 kHz and DFBIA is performed with 50 kHz and 200 kHz. TBW can be measured using SFBIA and TBW and ECW can be calculated by DFBIA. By measuring the impedance (Z_B) at 50 kHz and 200 kHz and by applying predictive equations (5a), (5b), (5c), and (6), both extracellular water (ECW) and TBW, respectively, are calculated and the intracellular water (ICW) is deduced [45]. The extra-cellular mass (ECM) and body cell mass (BCM) are found from ECW and ICW, respectively [45]. Several equations are proposed and used to predict fat-free mass (FFM). ECW can be found related to extracellular mass (ECM) and ICW to body cell mass (BCM). The equation for SFBIA and DFBIA is shown in (5a), (5b), (5c), and (6):

$$\text{TBW (Liters)} = \left[\frac{\left(0.3963 \times \text{height}^2\right)}{\text{impedance (50 kHz)}}\right] + \left(0.143 \times \text{weight}\right) + 8.4, \quad (6)$$

$$\text{ECW (Liters)} = \left[\frac{\left(0.178458 \times \text{height}^2\right)}{\text{impedance (5 kHz)}}\right] + \left(0.06895 \times \text{weight}\right) + 3.794, \quad (7a)$$

$$\text{TBW (Liters)} = \left[\frac{\left(0.24517 \times \text{height}^2\right)}{\text{impedance (200 kHz)}}\right] + \left(0.18782 \times \text{weight}\right) + 8.197. \quad (7b)$$

4. Electrical Impedance Spectroscopy (EIS)

Electrical impedance spectroscopy (EIS) [52–54] estimates the complex electrical impedance ($Z(f)$) and its phase angle ($\theta(f)$) of a subject under test (SUT) at different frequency points f_i (f_i:$f_1, f_2, f_3, \ldots, f_n$) by measuring the surface potentials ($V(f)$) developed for a constant current

injection ($I(f)$) at the boundary through a linear array of the surface electrodes attached to the SUT (Figure 9). In EIS, a frequency dependent constant amplitude sinusoidal current ($I(f)$) is injected through either two-electrode method or four-electrode method. As explained earlier, in 2-electrode based EIS and 4-electrode based EIS methods, the surface electrodes through which the current signal is injected are known as the current electrodes or the driving electrodes (as shown by the red colored electrodes in Figure 9) and the electrodes on which the frequency dependent ac potential ($V(f_i)$) is measured are called voltage electrodes or sensing electrodes (as shown by blue colored electrodes in Figure 9). Therefore, in EIS the frequency dependent electrical bioimpedance $Z(f_i)$ is found as the transfer function of the SUT, and thus the $Z(f_i)$ is calculated by dividing the voltage data ($V(f_i)$) measurement by applied current ($I(f_i)$) as shown in

$$Z(f_i) = \frac{V(f_i)}{I(f_i)}. \tag{8}$$

EIS can be potentially used as a nondestructive evaluation technique [55] for a number of applications in the field of science engineering and technology. The EIS-based frequency response studies on the electrical impedance of any material can provide its structural and compositional properties as well the frequency response of the material properties which can be potentially used for nondestructive material characterization [52–54]. Therefore the EIS has been suitably applied in several fields such as electrochemistry and chemical engineering [54, 56–61], material engineering [62–71], biomedical engineering [72–76], civil engineering [77–79], wood science [80, 81], plant physiology [82–84], microfluidics [85, 86], material engineering [87–90], fuel cell technology [91], and MEMS and thin films [92, 93] and so on.

5. Impedance Plethysmography (IPG)

Impedance plethysmography (IPG) is a electrical impedance based noninvasive medical diagnostic procedure which measures small changes in the blood volume in terms of its electrical bioimpedance of a body part, say chest, calf, or other regions of the body, to study the tissue health condition of the patient. The impedance measured in IPG provides the information about the tissue health of the body tissue, and hence it can be suitably used to indirectly study and analyze the tissue health and function of a patient under test. Therefore, the IPG can be considered as a bioimpedance analyzing technique that measures the change in blood volume for a specific body segment by measuring the electrical impedance which changes with a change in the blood volume.

5.1. IPG Procedure. In IPG, four conductive bands are taped around the body part or a limb and the limb impedance change due to the blood circulation is measured to calculate the blood volume changes (Figure 10(a)). A low amplitude, low frequency (50 kHz) ac current is passed through two outer electrodes and the change in electrical impedance is measured (Figure 10(b)) across the inner electrodes. In early

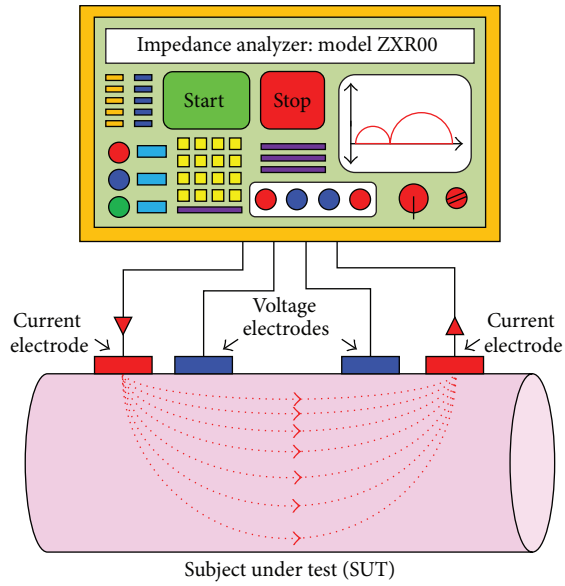

Figure 9: Electrical impedance spectroscopy (EIS) studies on biological materials with four-electrode technique using an impedance analyzer.

1950's, Nyboer [94, 95] proposed the impedance plethysmography equation to evaluate the volumetric change in the body parts in terms of impedance. But the formula proposed by Swanson and Webster, 1976 [96] is more simpler both mathematically and computationally. The formula works on three assumptions: the expansion in the artery is uniform, blood resistivity (ρ_b) does not change, and current fluxes are parallel to the artery (Figure 10(b)). In the theory of IPG, for each pressure pulse produced due to the blood flow through limb having an artery with an volume V and cross sectional area A, an extra amount blood with a volume of ΔV enters to that limb by increasing the limb volume from V to $V + \Delta V$ and consequently a shunting impedance (Z_b) is assumed to be produced. Therefore the (Z_b) is given by [96, 97]

$$Z_b = \rho_b \frac{L}{\Delta A}. \tag{9}$$

Hence, the artery volume change is given by [96, 97]

$$\Delta V = L \cdot \Delta A = \rho_b \frac{L^2}{Z_b}. \tag{10}$$

For each pressure pulse, the area of the artery (A) increases from A to $A + \Delta A$ (Figure 10). Consequently, the artery impedance (Z_b) is reduced by adding an impedance (ΔZ) produced by the ΔA and this Z_b will be connected in parallel to Z [96, 97].

As we measure the ΔZ rather that Z_b, the Z_b is required to be replaced by ΔZ. Now the blood impedance change, ΔZ, is given by [96, 97]:

$$\Delta Z = (Z_b \parallel Z) - Z = -\frac{Z^2}{Z + Z_b}. \tag{11}$$

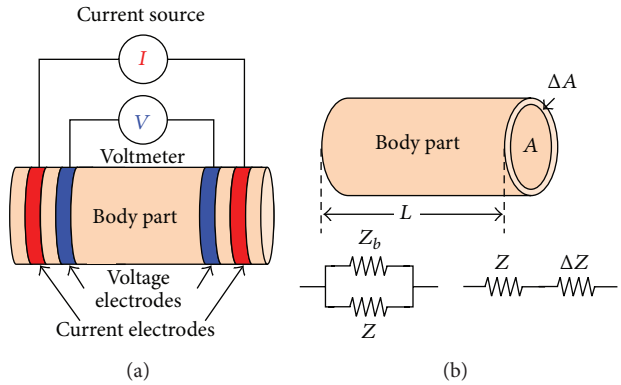

FIGURE 10: The schematic of the impedance measurement in IPG with four-electrode method and the calculation of limb volume in terms of bioimpedance: (a) impedance measurement of body part with four-electrode method, (b) volume change in body part due to blood pressure pulse and corresponding impedance variation due to the volume change.

Now as, $Z_b \gg Z$, the Z_b is given by [96, 97]:

$$\frac{1}{Z_b} \cong -\frac{\Delta Z}{Z^2}. \tag{12}$$

Therefore, the increases in the limb volume ΔV is given by [96, 97]:

$$\Delta V = -\rho_b \frac{L^2 \Delta Z}{Z^2}. \tag{13}$$

If all the assumptions are valid, then the volumetric change in a body part due to blood flow can be calculated from the impedance measurement using IPG technique.

Peterson [98] has conducted the experiments conducted on an impedance plethysmograph suitable for ambulatory blood pressure monitoring. The impedance plethysmograph, developed and used in the experiment worked as an ambulatory blood pressure monitor (ABPM), contained four circular copper band electrodes attached to the upper left forearm of a volunteer subject. In ABPM, the impedance was measured by using a signal generator connected to the outer two bands for electric current injection, and an amplifier circuit connected across the inner two electrodes for voltage measurement [98].

5.2. Advantages. Compared to the other techniques, the Impedance Plethysmography (IPG) has a number of advantages as listed below:

(i) noninvasive;

(ii) low cost;

(iii) fast process

(iv) portable and easy to operate and dry type testing procedure;

(v) bedside measurement and ambulatory measurement are possible;

(vi) measurement in ICU is possible;

(vii) current density in IPG with ring electrodes is more uniform compared to other four electrode methods using spot electrodes;

(viii) skin electrode impedance effect is less and skin impedance can be further reduced by applying the electrode gel;

(ix) electrical signal in IPG is easily to control, process and acquire;

(x) IPG is less temperature dependent;

(xi) surrounding humidity effect in IPG is less;

(xii) applicable for healthy persons and patients of all age groups;

(xiii) IPG helps doctors and clinicians to measure changes in venous blood volume as well as the arteries pulsations;

(xiv) compared to venography, which is invasive and requires a skilled person to perform and interpret accurately, IPG is an easy to perform and understand;

(xv) ICG helps a doctor to detect deep vein thrombosis (DVT);

(xvi) IPG is found 96% sensitive and 98% specific in the diagnosis of arterial occlusive disease and more than 85% sensitive in the diagnosis of DVT and valvular diseases.

5.3. Limitations. IPG has the following limitations:

(i) electric current is injected to the subject;

(ii) electro skin impedance error is introduced.

5.4. Applications. Due to the number of advantages of the IPG, it has been used for several application as follows:

(i) blood volume measurement;

(ii) detection of deep vein thrombosis (DVT);

(iii) detection of venous and arterial insufficiency;

(iv) screening of the patients who are likely to have blood clots in legs;

(v) detection of the source of blood clots in the lungs (pulmonary emboli);

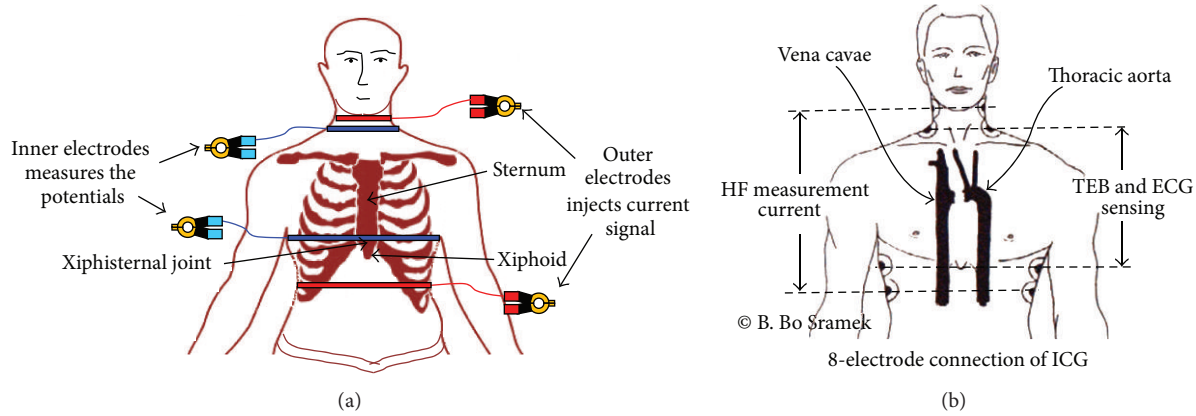

Figure 11: The schematic of the impedance measurement in ICG with four-electrode method: (a) impedance measurement with band electrode (photograph courtesy: Ref [100]) and (b) impedance measurement with band electrode (photograph courtesy: http://www.hemosapiens.com/teb.html (with permission of B. Bo Sramek), Retrieved on: 12.12.2013).

(vi) indirect assessment of central and peripheral blood flow;

(vii) detect blood flow disorders such as venous and arterial occlusive diseases (estimate severity);

(viii) early stage arteriosclerosis;

(ix) functional blood flow disturbances, migranes;

(x) general arterial blood flow disturbances.

6. Impedance Cardiography (ICG)

6.1. Introduction. Impedance cardiography (ICG), also referred to as transthoracic electrical impedance plethysmography, is a technology which calculates the changes in blood volume in transthoracic region over time in terms of the changes in transthoracic impedance (Figure 11) called thoracic electrical bioimpedance (TEB) or Z_o. Body impedance is changed in human body due to the blood circulation caused by each heart rhythms, and hence the transthoracic impedance (Z_o) is influenced by its biological composition, breathings, and by the blood circulation and blood volume in the transthoracic region. Therefore, analyzing the Z_o, the health of the heart along with a number of hemodynamic parameters can be evaluated. ICG has been researched since the 1940s. NASA developed the technology in the 1960s [99].

6.2. ICG Procedure. The ICG procedure is basically similar to the IPG procedure in which the impedance measurement is conducted by injecting a low amplitude constant alternating electric current (frequency range of 20 kHz–100 kHz) [58] into the volume conductor and measuring the corresponding voltage (Figure 11). The frequency dependent impedance $Z(f)$ is measured from the ratio of voltage $V(f)$ to current $I(f)$ applied, usually the DC value is eliminated, and only the impedance variation ΔZ is further examined [100]. The current injection and the voltage measurement are conducted with four-electrode method either using the ring electrode or the spot electrodes (common ECG electrodes). In ring electrode based ICG system, four ring electrodes are required, whereas the ICG with spot electrode configuration needs eight ECG electrodes. Hence, all the ICG systems are operated with four-electrode measurement technique using either four-band electrodes (Figure 11(a)) or 8 spot electrodes (Figure 11(b)). The 4-electrode and 8-electrode connections of ICG are shown in Figures 11(a) and 11(b), respectively. In ring electrode connection, one electrode of the driving electrodes (the outer pair) is placed around the abdomen and the other is placed around the upper part of the neck (Figure 11(a)). For the sensing electrode pairs (inner electrode pair), one electrode is placed around the thorax at the xiphisternal joint and the other around the lower part of the neck (Figure 11(a)). In 8-electrode connections of ICG also the current injection and voltage measurement are conducted using four-electrode method as the current is injected through the two upper most electrodes and two lower most electrodes and the voltage data are collected across the inner two sets (each set contains two spot electrodes) of the electrode. In recent times the band electrodes are often replaced with spot electrodes such as normal ECG electrodes [100]. A low magnitude, low frequency ac signal, is injected by current (red in the figure) electrodes. Voltage developed across voltage electrodes due to the current injection through the current electrodes is measured and the average transthoracic impedance (Z_o) across the transthoracic region and the small change in impedance (ΔZ) due to blood flow are calculated and monitored against time. After getting the Z_o, dZ/dt, ΔZ are calculated. Analyzing the Z_o, dZ/dt, ΔZ, the stroke volume, cardiac volume, and several hemodynamic parameters are calculated for noninvasive diagnosis of the heart and circulatory system.

Figure 12 shows a typical thorax impedance curve (Z), its first time derivative (dZ/dt), the simultaneous electrocardiogram (ECG), and phonocardiogram (PCG) curves [100]. It is important to note that a decrease in impedance results in an increase in the y-axis magnitude, and hence this sign convention describes the changing transthoracic admittance.

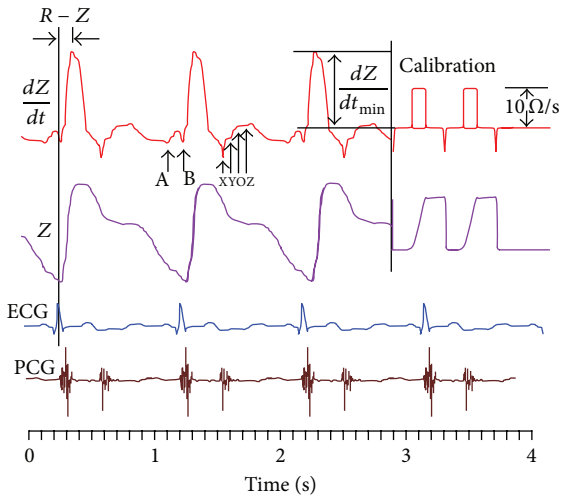

FIGURE 12: The transthoracic impedance curve [100] over time.

Thus a decrease in impedance can be explained by an extra amount of blood (low impedance material) flow in the thorax. It is also important to note that the polarity of the first derivative curve (dZ/dt) is consistent with the impedance (Z) curve.

6.3. ICG and Hemodynamic Parameters. In ICG, a number of hemodynamic parameters are derived to study the hemodynamic health and functions including the following:

(i) stoke volume;
(ii) cardiac volume;
(iii) stroke volume/stroke volume index (SV/SVI);
(iv) cardiac output/cardiac index (CO/CI);
(v) systemic vascular resistance/index (SVR/SVRI);
(vi) velocity index (VI);
(vii) thoracic fluid content (TFC);
(viii) systolic time ratio (STR);
(ix) left ventricular ejection time (LVET);
(x) preejection period (PEP);
(xi) left cardiac work/index (LCW/LCWI);
(xii) heart rate (HR).

6.3.1. Hemodynamic Parameter Calculation. The following section represents the detail explanations and the formula of the hemodynamic parameters [100, 101].

Stroke Volume. Stroke volume is very important in cardiovascular physiology to determine the cardiac function and cardiac health and cardiac parameters such as cardiac output (CO), ejection fraction (CEF) and so forth Stroke volume is measured in milliliters per beat (mL/beat) which is almost equal for each ventricles (approximately 70 mL/beat for a normal adult subject). SV is indexed to a patient's body size by dividing by body surface area (BSA) to yield stroke index (SI). Using the information acquired from the echocardiography for a given ventricle, the SV is estimated by subtracting volume of the blood in the ventricle at the end of a beat (called end-systolic volume or ESV) from the volume of blood just prior to the beat (end-diastolic volume or EDV). Using the impedance method, the SV is calculated by the formula as described below.

(i) stroke volume = $[\rho]\times [L/Z_o]^2 \times \Delta Z$ (Nyboer Formulae);
(ii) stroke volume = $[\rho] \times [L/Z_o]^2 \times dZ/dt \times$ LVET (Kubicek Formulae);
(iii) stroke volume = $[V/Z_o] \times dZ/dt \times$ LVET (Sramek Formulae),

where ρ is specific resistivity of blood which is a constant for a particular subject, L is transthoracic length, Z_o is average transthoracic impedance, LVET is left ventricular ejection time, V is volume of the transthoracic tissues involved electrically during the test = $L^3/4.25$.

Cardiac Volume. The cardiac volume refers to the volume of the heart which is usually relating to the volume of blood contained within it at various periods of the hear cycle.

Cardiac Output (CO). Cardiac output (CO) is the total amount of blood ejected or pumped out by the left ventricle of the heart into the systemic circulation in one minute. Hence the CO is found as equal to the stroke volume times the heart rate. Using the cardiac output of a human subjects, one more hemodynamic parameter, called the cardiac index (CI), is calculated by dividing the CO by the body surface area (BSA). The CO is measured in (L/min or mL/min) and as the CI is measured in litres per minute per square metre (L/min/m^2). The CO is, generally, found as approximately 5.6 L/min for a human male subject and 4.9 L/min for a human female subject. Thus the CO and the CI are found as:

CO = (stroke volume × heart rate);

CI = cardiac output/body surface area.

6.4. Advantages. The impedance cardiography (ICG) has a number of following advantages:

(i) noninvasive, low cost, fast, portable, safe;
(ii) current distribution is better; and less noise effect;
(iii) electrode-skin impedance effect being less.

7. Electrical Impedance Tomography (EIT)

7.1. Introduction to EIT. Electrical impedance tomography (EIT) [102–114], a computed tomographic image reconstruction technique, is a nonlinear inverse problem in which the electrical conductivity or resistivity of a conducting domain (Ω) is reconstructed from the surface potentials developed by a constant current signal injected (Figure 13) at the domain boundary ($\partial\Omega$). A low frequency, constant amplitude sinusoidal current is injected to the boundary ($\partial\Omega$) of the object domain (Ω) to be imaged within a volume

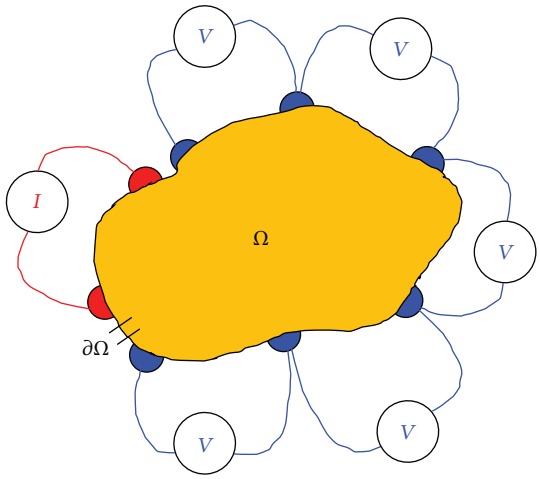

FIGURE 13: A closed domain of interest under EIT scanning with a constant current injection through driving electrodes and boundary potential measurement on sensing electrodes.

conductor surrounded by an array of surface electrodes and the boundary potentials are measured using an electronic instrumentation [115–123]. Constant current signal is injected to the closed domain under test (DUT) through the different pairs of electrodes called driving electrodes and the voltage data are collected from the other electrodes or electrode pairs called sensing electrodes, and the set of voltage current data obtained from this noninvasive boundary measurements is used to reconstruct the conductivity distribution of the DUT. Boundary data are then sent to the PC and the data are processed in PC to reconstruct the spatial distribution of the electrical conductivity of the DUT using a computer program called image reconstruction algorithm [124–133].

EIT is a low cost, portable, fast, noninvasive, nonionizing, and radiation free technique, and hence it is found advantageous in several fields of applications application compared to the other computed tomographic methods like X-ray CT [134–136], X-ray mammography [137], MRI [138, 139], SPECT [140, 141], PET [142, 143], ultrasound [144, 145], and so forth. EIT has been applied in a number of research areas such as medical imaging clinical diagnosis [146–152], chemical engineering [153], industrial process application [154, 155], material engineering [156], microbiology and biotechnology [157, 158], nondestructive testing (NDT) in manufacturing technology [159], civil engineering [160], earth science and geophysics and geoscience [161], defense fields [162], archaeology [163], oceanography [164], environmental engineering [165], and other fields of applied science, engineering and technologies [166].

7.2. Physics of EIT. In EIT, when a constant current is injected into DUT, the current signal conducted through the domain produces current fluxes which induce potentials within the DUT. The potential profiles developed by the current conduction depend on the profiles of the current fluxes which are influenced by the impedance profile of the DUT. As the profile of the current conduction in a homogeneous domain (Figure 14(a)) differs from the current flux lines produced by the inhomogeneous DUT (domain with inhomogeneity) (Figure 14(b)), the voltage profile of the homogenous DUT will be different from the domain with inhomogeneity. Similarly, the boundary potential profiles will depend on the domain impedance distribution, and hence the information of the impedance distribution of the DUT is hidden inside the boundary potential data.

7.3. Comparison with CT. EIT is a computed tomographic imaging modality which uses an electrical energy (either by injecting electrical current or voltage signals) and the developed potentials are collected at the domain boundary, whereas in X-ray CT, X-ray beams are passed through the SUT at different angles, called the projection angles, and the attenuated X-ray beams are collected by the X-ray detectors. The image reconstruction algorithm uses the measured data in PC and reconstructs the spatial distribution of the electrical impedance and the X-ray attenuation coefficient of the SUT in EIT and CT, respectively. Therefore, the CT is a tomographic technique imaging with X-rays and EIT reconstructs the tomographic images with electric current.

7.4. Advantages of EIT. EIT has several advantages over other computed tomographic imaging techniques used for medical imaging applications as summarized below:

(i) noninvasive;
(ii) radiation free;
(iii) nonionizing method;
(iv) fast data acquisition;
(v) high temporal resolution;
(vi) medically safe process;
(vii) low cost device;
(viii) portable device and easy to use;
(ix) suitable for bedside measurement and ICU monitoring;
(x) suitable for ambulatory monitoring;
(xi) negligible patient preparation is required;
(xii) no precautions are required;
(xiii) no postexperimental discomfort;
(xiv) no postexperimental precautions and restrictions;
(xv) suitable for the patients of any age groups as well as critically ill patients.

7.5. Capacitance Tomography and Resistance Tomography. In EIT the spatial distribution of the electrical conductivity is reconstructed from the boundary data collected by an alternating current injection at the domain boundary. In some applications the electrical permittivity of the DUT is reconstructed from the voltage current data collected at the boundary and the imaging modality is called electrical capacitance tomography (ECT) [125, 133, 167, 168] which is

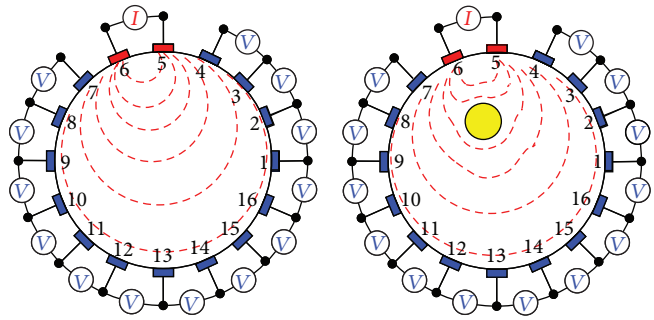

Figure 14: Variation in boundary data profiles for a homogeneous domain and a inhomogeneous domain (a domain with inhomogeneity) due to the variation in the profiles of impedance distributions (a) domain without inhomogeneity, (b) domain with inhomogeneity.

generally used in industrial process application and mechanical and material engineering. The electrical resistivity of the domain under test is sometimes reconstructed from the boundary data generated by a direct current injection in industrial process imaging, civil structure imaging, subsurface imaging, and other applications of geotechnology. This method is known as the electrical resistance tomography (ERT) [169–173].

7.6. Difference EIT and Static EIT. EIT image reconstructions are conducted from the boundary data either with the difference or dynamic imaging modality called the difference imaging or another modality called static imaging. In difference imaging, the impedance distribution of the DUT is reconstructed by comparing the data collected from the domain with inhomogeneity and the data collected from the homogeneous domain (reference data), whereas the static imaging reconstructs the conductivity distribution from the data collected from the inhomogeneous medium without using the reference data set. The present EIT technologies are generally found applied in difference imaging modalities as the static imaging seems to be difficult and more influenced by the measurement errors, and hence the static EIT is found still far from clinical applications primarily. Though the static EIT is found difficult due to the fundamental ill-posedness of the EIT inverse problem, but still it is little bit too early to say that the static EIT is not to be pursued since active researchers are still looking for innovative algorithms and new measurement technologies.

The dynamic or difference EIT that was introduced by Barber and Brown in 1984 [174] produces differential images, whereas the static imaging yields absolute images. The difference impedance imaging may be either the time difference EIT [105, 175, 176] or frequency difference EIT [105, 177, 178]. The time difference EIT imaging produces the images of the variation of the conductivity distribution of a region between two different time intervals [104, 179], whereas the frequency difference imaging reconstructs the impedance distribution from two data sets collected at two discrete frequencies. The difference EIT allows us to monitor the changes such as gastric emptying or long-term observation of body functions/volume changes [104, 179] including the visualization of physiological activities in a human body such as respiration. It can also be used for breast cancer detection, cardiac circulation, brain function, stomach emptying, fracture healing, bladder filling, and others. Difference EIT can also be used in nonmedical applications such as in corrosion detection, crack detection, electric field sensing, bubble detection, and other nondestructive testing.

7.7. Multifrequency EIT System. As the different biological tissues have different frequency versus impedance responses [5, 76, 180, 181], the multifrequency EIT [182–185] is found more effective and efficient in biological tissue characterization, medical imaging, and clinical diagnosis of the human diseases. The multifrequency EIT provides a lot of information about the tissue health which can be potentially utilized for better tissue characterization. Moreover, the multifrequency EIT can provide all the parameters in the frequency domain which adds another advancement in the diagnosis and treatment of the disease. Thus, the multifrequency impedance imaging can be suitably applied in diagnosis and treatment of the human diseases, tumors, lesions, and cancers.

7.8. 3D EIT. 2D electrical impedance tomography (2D-EIT) reconstructs the approximate spatial distribution of the internal impedance profile of a DUT from the boundary measurements of voltage-current data developed by a constant current injection through the surface electrodes fixed in a 2D plane within the patient's body [104]. Thus, the 2D EIT approximately reconstructs the 2D conductivity distribution by assuming the electrical current conducts in a 2D plane. But as the electrical current is not confined in the plane of electrode array rather it spreads over a 3D space within the volume conductor, the 2D EIT suffers from the errors contributed by this 3D conduction of electrical current [104]. Moreover, 2D EIT of a tissue under test provides only the 2D impedance distribution in its tomograms in which the 3D anatomical and physiological information is not available. But, 3D EIT provides 3D conductivity distribution with a better and more scientific visualization of the tissue interiors which helps the doctors and clinicians with better tissue characterization [104].

7.9. A Basic EIT System. A basic EIT system contains three parts (Figure 15): EIT instrumentation [115–123], a PC with reconstruction algorithm [124–133], and an array of EIT sensors or surface electrodes [57, 102, 106, 110, 186] attached to a practical phantom or a subject under test (SUT).

In EIT, an array of sensors or surface electrodes [57, 102, 106, 110, 186] is attached to the boundary of the DUT. A low frequency sinusoidal current of constant amplitude is generated by a constant current source and it is injected through the driving electrodes and the boundary potentials are measured on the sensing electrodes using a particular current injection and voltage measurement fashion called the current pattern [100, 187, 188]. Boundary potentials are measured using a data acquisition system (DAS) [108, 121, 123] and the processed data obtained from the data processing circuit containing amplifier and filters (Figure 15) are sent to the PC for computation and image reconstruction. Thus a basic EIT system has three main parts:

(i) EIT-instrumentation;

(ii) PC with reconstruction algorithm;

(iii) electrode array or EIT sensors attached to the subject under test (SUT).

7.10. EIT Instrumentation. A common EIT Instrumentation has four main parts:

(i) constant current injector (CCI);

(ii) signal conditioner block (SCB);

(iii) electrode switching module (ESM);

(iv) data acquisition system (DAS).

Constant current injector (CCI) may be developed with a signal/function generator and a voltage controlled current source (VCCS) which is used to inject a constant current signal to the domain boundary through the driving electrodes. The developed voltage signals on the sensing electrodes are processed by signal conditioner block (SCB) and sent to the DAS for data acquisition. The boundary data are collected with a particular current pattern by switching driving and sensing electrode in a particular fashion using a electrode switching module (ESM). The boundary data collected from a complete EIT scan of the object are sent to the PC for image reconstruction.

7.11. Electrode Array or EIT Sensors. Surface electrode array is a very important part of an EIT system as the boundary data quality, and thus the image quality depends on it. As the EIT electrodes are used to inject current to the body under test and collecting the voltage data at boundary electrodes, electrode parameters are very crucial in EIT imaging. For designing a better EIT electrode system, one should carefully select the electrode parameter such as electrode number, electrode material, electrode geometry (shape and size), electrode model (point, gap, shunt, and complete) or electrode type (noncompound or compound).

7.12. Reconstruction Algorithm. Image reconstruction algorithm is one of the most important parts of EIT system as the image reconstruction is conducted by the algorithm. The boundary potential data collected from the real objects (SUT) are sent to the PC and are processed to reconstruct the EIT images using the EIT reconstruction algorithm. EIT image reconstruction algorithm has generally two main parts:

(i) forward solver (FS);

(ii) inverse solver (IS).

The forward solver solves the characteristic equation or governing equation of EIT [102–110, 189–194] and computes the boundary potentials called calculated boundary data (V_c) for a known constant current simulation [C] in PC. The calculated potential data (V_c) are then compared with the measured potential data (V_m) in inverse solver (IS) and the conductivity distribution of DUT is reconstructed for which the difference between V_m and V_c ($\Delta V = V_m - V_c$) is minimized.

The Gauss-Newton based EIT image reconstruction algorithm (GN-EIRA) is generally developed with a finite element method (FEM) [189–196] based forward solver (FEM-FS) a Gauss-Newton based inverse solvers (GN-IS) in MATLAB. The GN-EIRA is developed with Gauss-Newton based minimization algorithm (GNMA) and Newton Raphson iterative technique (NRIT) [189–196]. The forward solver generally applies a numerical technique like FEM or boundary element method (BEM) [196] or else and calculates the nodal potentials [195] within the discretized domain. Using the forward solution data, the algorithm construct the sensitivity matrix, called Jacobean (J) which is used by the inverse solver. The inverse solver uses the voltage difference vector (ΔV) and J and calculates a correction or update in conductivity distribution to modify it for minimizing the voltage data mismatch. Inverse solver repetitively solves the forward solution and tries to compute an approximate conductivity distribution for which the difference between measured and calculated voltage data is minimized.

7.12.1. GN-EIRA. In EIT, the GN-EIRA is developed with a FEM based forward solver (FS) and Gauss-Newton method based inverse solver (GNIS), whereas the GNIS is developed with Gauss-Newton based minimization algorithm (GNMA) and Newton Raphson Iterative technique (NRIT). The forward solver solves the EIT governing equation by developing the forward model of the EIT problem and calculates the boundary potentials (V_c) for a known current injection [C] applied to the boundary of the domain with a known conductivity distribution [σ_0]. The solution obtained from the FP is also used to compute the potential mismatch vector [$\Delta V = V_m - V_c$] and the Jacobian (J) that are used in inverse problem to compute the conductivity update vector [$\Delta\sigma$]. The GNIS solves the inverse problem (IP) using the boundary data [V_c] computed by the forward solver and tries to estimate the domain conductivity distribution from measured boundary potential data (V_m) developed for the real current injection of the same amplitude. The GNIS in EIT repetitively calculates the conductivity update

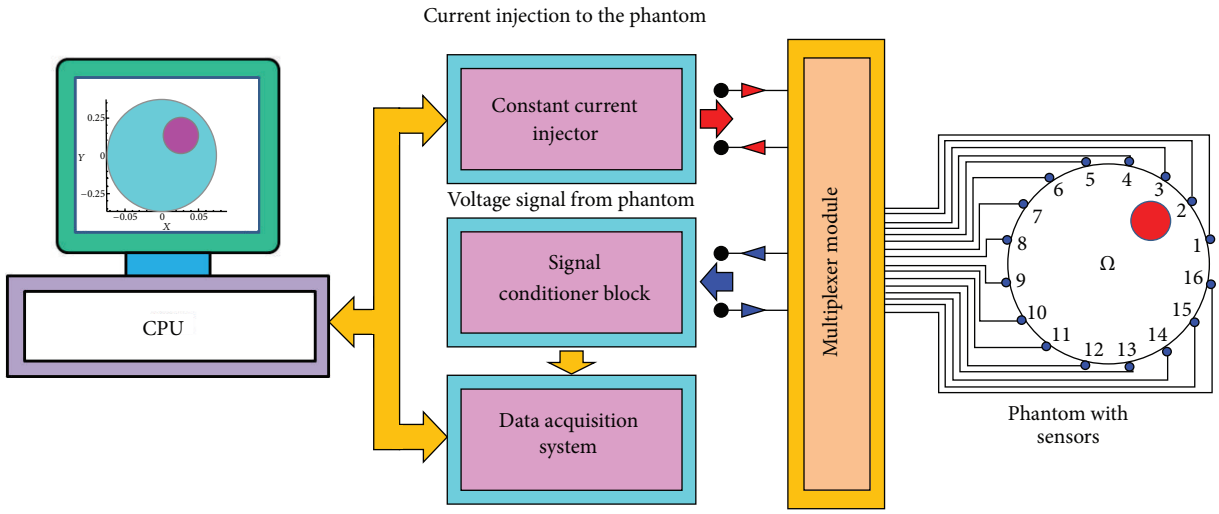

FIGURE 15: Schematic of a basic EIT system with patients with surface electrodes attached to its transthoracic region for thoracic imaging.

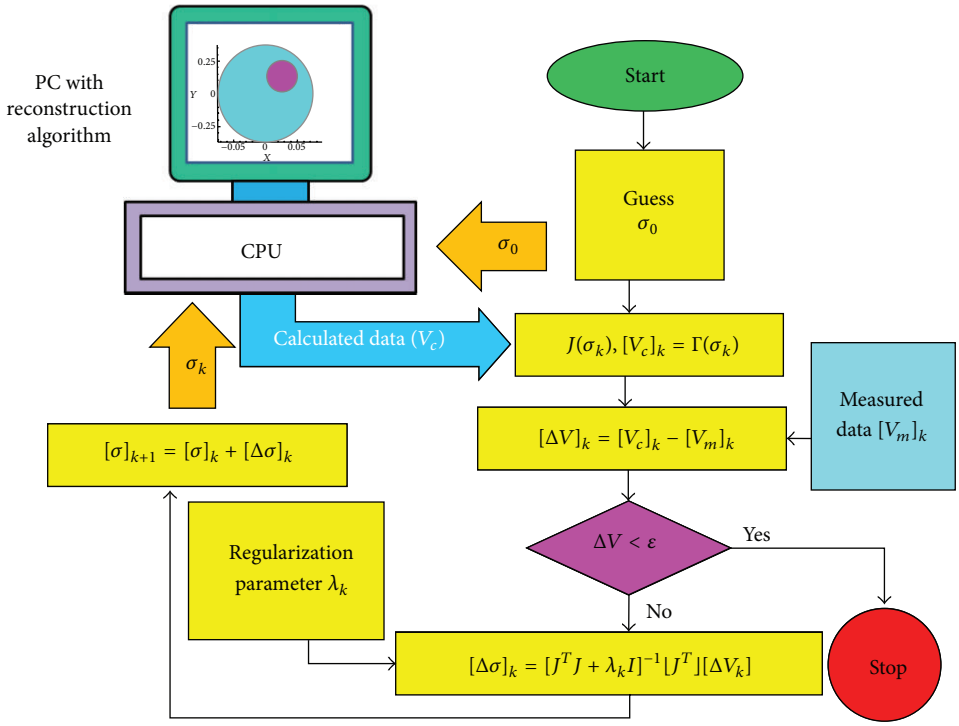

FIGURE 16: The flow chart of a standard EIT imaging reconstruction algorithm.

$[\Delta\sigma]$ vector and simultaneously reconstructs the conductivity distribution $[\sigma]$ in each iteration by updating the conductivity distribution obtained in previous iteration. The iteration process is continued to update the conductivity distribution with modified NRIT until a specified error limit criterion ($\varepsilon = f(\Delta V)$) is obtained (Figure 16).

7.12.2. Governing Equation of EIT. The EIT reconstructs the conductivity of a closed domain from the boundary voltage current data using the relationship of the domain conductivity distribution and the domain potentials distribution which is called the EIT governing equation. In EIT, the conductivity distribution of a DUT could be defined with the distinct values of electrical conductivities at each points within the domain which are associated with their corresponding coordinates. Now, if an electric current of constant amplitudes is injected to the domain boundary ($\partial\Omega$), the current flux will develop a particular potential profile within DUT. The developed potential profile will be the function of the current amplitude and the conductivity profile of the domain. Therefore, the "EIT governing equation" could be obtained as the relationship between the elemental electrical

conductivity (σ_e) of the domain and their corresponding potential values (Φ) using the Maxwell's equations. EIT governing equation can be represented as a partial differential equitation [102–110, 189–195] as shown in

$$\nabla \cdot \sigma \nabla \phi = 0. \tag{14}$$

7.12.3. Boundary Conditions. The forward solver of EIT reconstruction algorithm discretizes the DUT with a finite element mesh containing a finite number of triangular elements and the finite number of nodes and applies the FEM formulation technique on the EIT governing equation (14) of the DUT. As the EIT governing equation is a nonlinear partial differential equation, it has an infinite number of solutions, and hence, to restrict its solutions space, the FEM based EIT forward solution process essentially needs the boundary conditions [1–5] which provide some specified value of certain system parameters which may be either the potentials at the surface or the current density crossing the boundary or mixed conditions.

The boundary conditions, in which the parameters are the potential at the domain boundary ($\partial\Omega$), are named as the Dirichlet boundary conditions which are represented as [102–110, 189–196]

$$\Phi = \Phi_i, \tag{15}$$

where $i = 1, \ldots, d$ are the potentials on the nodes under electrodes (d is number of electrodes potentials).

On the other hand, the boundary conditions of EIT which specify the current density crossing the boundary ($\partial\Omega$) are known as the Neumann boundary conditions [102–110, 189–196] defined as:

$$\int_{\partial\Omega} \sigma \frac{\partial \Phi}{\partial n} = \begin{cases} +I & \text{on the source electrode} \\ & (I \text{ is the injected current amplitude}), \\ -I & \text{on the sink electrode} \\ & (I \text{ is the injected current amplitude}), \\ 0 & \text{otherwise.} \end{cases} \tag{16}$$

7.12.4. Forward Solution. In EIT, the FS derives the forward model of a DUT from its governing equation by applying the FEM formulation technique on (1) and imposing the boundary conditions. Using the initial guessed conductivity distribution [σ_0] and nodal coordinates, the FS develops the forward model which is a system of equations represented in the form of a matrix equation (17). The forward model, in form of the matrix equation, actually represents the relationship between the current injection matrix [C] (matrix of the applied current signal) and the nodal potential matrix [Φ] (matrix of the developed nodal potential data) through the transformation matrix [$K(\sigma_e)$] as given below [102–110, 189–195]:

$$[\Phi] = \left[K\left(\sigma_e\right)\right]^{-1} [C], \tag{17}$$

where σ_e is the elemental conductivity distributions.

The FS in EIT thus develops the forward model of the DUT and calculates the boundary potential (V_c) data for a known conductivity distribution (initial guess), [$\sigma_e = \sigma_0$], and a known simulated current injection [C] (available from the boundary conditions).

7.12.5. Inverse Solution. If F is a function mapping an e dimensional (e is the number of element in the FEM mesh) impedance distribution into a set of d (d is the number of the experimental measurement data ([V_m]) available) approximate measured voltages, then the conductivity of the DUT can be estimated from the boundary data by applying the Gauss-Newton method based minimization algorithm [102–110, 189–195] which tries to find a least square solution of the minimized object function s_r [102–110, 189–195] which is defined as

$$\begin{aligned} s_r &= \frac{1}{2}\left\|V_m - F\right\|^2 + \frac{1}{2}\lambda \left\|R\sigma\right\| \\ &= \frac{1}{2}\left(V_m - F\right)^T \left(V_m - F\right) + \frac{1}{2}\lambda (R\sigma)^T (R\sigma)^2, \end{aligned} \tag{18}$$

where F represents the forward model predicted boundary potential data or V_c, R is a matrix which is called the regularization matrix operator, and λ (positive scalar) is called the regularization coefficient or regularization parameters [102–110, 189–195].

Thus, the Gauss Newton method based minimization technique of EIT image reconstruction algorithm gives the conductivity update vector [$\Delta\sigma$] as

$$\Delta\sigma = \frac{s_r'}{s_r''} = \frac{\left(F'\right)^T \left(V_m - F\right) - \lambda (R)^T (R\sigma)}{\left(F'\right)^T \left(F'\right) - \left(F''\right)^T \left(V_m - F\right) + \lambda R^T R}. \tag{19}$$

Now, neglecting the higher order matrix $[f'']^T$ in (19), called the "Hessian matrix," and replacing the matrix [F'] by the sensitivity matrix of the system [J], called the "Jacobian matrix" of the system, the conductivity update vector [$\Delta\sigma$] reduces to

$$\Delta\sigma = \frac{J^T \left(V_m - f\right) - \lambda I\sigma}{J^T J + \lambda I}, \tag{20}$$

where the matrix [I] represents the identity matrix which is equal to [R^T][R].

Therefore, the GN-EIRA of the EIT provides the general solution of the conductivity distribution of the DUT at the kth iteration of the algorithm as

$$\left[\sigma_{k+1}\right] = \left[\sigma_k\right] + \left[\left[J^T J + \lambda I\right]^{-1} \left[J^T \left[V_m - f\right] - \lambda I\sigma\right]\right]_k. \tag{21}$$

7.13. Subject Under Test (SUT) in EIT. The subject to be imaged or subject under test (SUT) in EIT may be a human subject (healthy human volunteer or a patient) or laboratory animal or a tissue mimicking model object called "practical phantom" [117, 129, 131, 186, 188, 197–202]. The EIT instrument, called electrical impedance tomograph, is applied to the SUT and the EIT imaging is conducted for the domain

of interest or domain under test (DUT) at a particular plane within the SUT in 2D or for a number of parallel 2D EIT domains called image slices in 3D EIT.

7.13.1. Practical Phantoms. EIT phantoms [117, 129, 131, 186, 188, 197–202] which are the mimic models of the human body tissue or human body parts are essentially required to assess the performance of electrical impedance tomography (EIT) systems for their validation, calibration, and comparison purposes. EIT phantoms are classified mainly into two types, namely, network phantoms [201, 203–209] and real object phantoms [115, 186, 187, 198–200, 202, 210–215]. Real object phantoms are developed with a phantoms tank filled with two or more objects (biological or nonbiological) with different conductivities surrounded by an array of surface electrodes [97] housed on the inner wall of the phantom tank. Researchers have reported several types of real object phantoms for studying their EIT systems such as saline-insulator phantoms [115, 186, 187, 210–215], saline-agar phantom [216–218], saline-vegetable phantom [198, 212, 215, 219, 220], and passive or active element phantoms [200, 221]. All the phantoms have their own advantages and disadvantages. Network phantoms are developed with circuit elements housed on a electronic element base or printed circuit board (PCB). Network phantoms do not require any surface electrodes; only electronic connections are sufficient to interface the phantom with the EIT instrumentation. Though the network phantoms with electrical components are sometime advantageous for their long life, rigidity, stability, and ease of control, yet these phantoms fail to provide a mimic model the real biological tissue or the real body parts.

7.13.2. Disadvantages of Saline Phantoms. Saline phantoms with solid inorganic (plastic, wood, or metal rod) or organic (vegetables or other biological tissues) materials are very popular in EIT as they are low cost and easy to develop and can be developed with rigid or flexible tanks of any shape and size. However, they cannot be assumed as a perfect mimic of the body parts as the background medium is a pure saline solution (purely resistive), whereas none of the human body parts are purely resistive in nature. Also, it is quite difficult to reconstruct the actual resistivity of the insulator inhomogeneity in a saline background because of their large resistivity difference. As the frequency versus impedance response of the saline solution is constant, the saline phantom fails to present a mimic model of body tissue as the response of the real tissue varies with frequency according to their physiological and physiochemical compositions contributing to a complex bioelectrical impedance. Moreover, the evaporation of the saline solution makes them unstable over the time which makes the assessment erroneous in real case. Hence the saline phantoms and the phantoms with circuit elements sometimes fail to calibrate the multifrequency EIT systems and the medical EIT systems. It is found that the practical biological phantoms consisting two different materials with low resistivity difference, such as the real tissue phantoms [188, 197, 200], are more suitable for multifrequency impedance imaging studies.

7.14. Scope and Challenges in EIT. Though the EIT technology has been studied in different fields of science and technology, yet EIT has shown its several advantages in medical imaging, and hence a number of research groups are working on it for medical and clinical imaging purposes. Although, due to poor signal to noise ratio (SNR) [222–225], of the boundary potential data and poor spatial resolution [226–228] the EIT technology has a lot of scope to work on it and a number of technical challenges to be solved. Therefore, though a medical EIT system has a number of advantages over the available regular medical imaging modalities, and the technical challenges and research scope of EIT technology have ever attracted the researcher to work for improving EIT reconstruction. A lot of research opportunities are still there in absolute impedance imaging, high speed reconstruction, improved 3D reconstruction, and spatial resolution of EIT.

8. Present Status and Future Directions of Impedance Methods

Multifrequency bioelectrical impedance analysis (BIA) [229, 230] is found as one of the core interest among the researchers in the field of bioelectrical impedance. A part of the researchers are studying on the instrumentation who are developing more sophisticated instrumentation. The future studies may be conducted on the wireless and Bluetooth based instrumentation for BIA techniques. Among the multifrequency impedance analyzing techniques EIS is the most popular and strong method. EIS methods are now being studied with a pulsed signal based EIS instrumentation [231–233] for tissue characterizations as well as single cell analysis [231–233]. The wireless and Bluetooth based instrumentation for EIS techniques can also be implemented in future studies. Presently the IPG is being studied for finger plethysmography [234, 235] by J. G. Webster group in University of Wisconsin, Madison, USA. J. G. Webster group is also working on the automated IPG instrumentation and the modern software based IPG systems [236–238]. In future, the wireless and Bluetooth based instrumentation for IPG techniques can also be implemented. ICG has several advantages in cardiac parameter assessment over the other conventional invasive methods. In recent years the ICG instruments are available from few industry-institute research collaborations. ICG can be studied as multifrequency bioimpedance methods for transthoracic parameter assessment for better cardiac health monitoring. ICG can also be studied as an ambulatory monitoring or long-term monitoring modality in intensive care unit (ICU). The electrical behavior of biological tissue is very complex, and hence, though the BIA, EIS, IPG, ICG are found with some successful applications, yet the EIT has not yet been considered as the regular medical imaging modality. Nonlinearity, ill-posedness, modelling error, measurement error, and other challenges are still required to be overcome. But, due to some unique advantages, if these challenges are overcome by future research on EIT, it may be also applied more effectively and efficiently compared to the other imaging modalities which are now being commonly used in some particular medical applications like brain imaging

[239–241], breast imaging [242–249], abdominal imaging [250–252], whole body imaging [253–256], and so forth. Therefore, the EIT technology has a lot of potentials for low cost fast tomographic imaging, though the problems of low spatial resolution and poor signal to noise ration of the system should be solved in future research. Absolute conductivity imaging, better electrode performance, accurate system modelling, and high speed 3D EIT are also to be explored more to improve the EIT technology.

9. Conclusions

Bioelectrical impedance methods used for noninvasive health monitoring are reviewed in detail in this paper. The paper reviewed the technical aspects of some major bioimpedance methods such as bioelectrical impedance analysis (BIA), electrical impedance spectroscopy (EIS), electrical impedance plethysmography (IPG), impedance cardiography (ICG), and electrical impedance tomography (EIT). Detailed discussions on the theoretical aspects, working principles, applications, advantages, limitations and present research scenario, future trends, and challenges of these bioimpedance methods have been presented in detail in this paper. It is found all the methods are comparatively low cost, fast, portable, and simple. All the methods have a number of advantages in their application for the noninvasive investigations compared to the other methods, and hence they have been potentially applied for noninvasive diagnosis of tissue health. BIA, EIS, IPG, and ICG have been successfully studied by a number of researchers and scientists over past few decades for assessing a number of tissue parameters and the tissue compositions for tissue health diagnosis. BIA, EIS, IPG, ICG, and EIT have been used for biological tissue characterization by utilizing the electrical impedance information. BIA, EIS, IPG, and ICG study the tissue properties in terms of the lump impedance parameters at a particular frequency or at different discrete frequencies obtained from the boundary voltage current measurement. On the other hand the EIT provides a spatial distribution of the impedance profile of a 2D or 3D domain under test using a set of boundary voltage-current data. In this regard, EIT provides more information about the tissue physiology and pathology, and hence it has more potential in several applications. The paper presents a clear and detailed technical overview of BIA, EIS, IPG, ICG, and EIT methods and their applications for noninvasive tissue characterization and tissue health diagnosis which will help the readers to get the clear technical perspectives of these impedance analyzing techniques.

Conflict of Interests

The author declares that there is no conflict of interests regarding the publication of this paper.

References

[1] F. H. Netter, *Atlas of Human Anatomy, Rittenhouse*, Book Distributors Inc, 2nd edition, 1997.

[2] J. J. Ackmann, "Complex bioelectric impedance measurement system for the frequency range from 5 Hz to 1 MHz," *Annals of Biomedical Engineering*, vol. 21, no. 2, pp. 135–146, 1993.

[3] J. J. Ackmann and M. A. Seitz, "Methods of complex impedance measurements in biologic tissue," *Critical Reviews in Biomedical Engineering*, vol. 11, no. 4, pp. 281–311, 1984.

[4] K. Cha, G. M. Chertow, J. Gonzalez, J. M. Lazarus, and D. W. Wilmore, "Multifrequency bioelectrical impedance estimates the distribution of body water," *Journal of Applied Physiology*, vol. 79, no. 4, pp. 1316–1319, 1995.

[5] T. K. Bera and J. Nagaraju, "Electrical impedance spectroscopic study of broiler chicken tissues suitable for the development of practical phantoms in multifrequency EIT," *Journal of Electrical Bioimpedance*, vol. 2, pp. 48–63, 2011.

[6] A. D. Bauchot, F. R. Harker, and W. M. Arnold, "The use of electrical impedance spectroscopy to assess the physiological condition of kiwifruit," *Postharvest Biology and Technology*, vol. 18, no. 1, pp. 9–18, 2000.

[7] E. C. Hoffer, C. K. Meador, and D. C. Simpson, "Correlation of whole-body impedance with total body water volume," *Journal of Applied Physiology*, vol. 27, no. 4, pp. 531–534, 1969.

[8] H. C. Lukaski, P. E. Johnson, W. W. Bolonchuk, and G. I. Lykken, "Assessment of fat-free mass using bioelectrical impedance measurements of the human body," *American Journal of Clinical Nutrition*, vol. 41, no. 4, pp. 810–817, 1985.

[9] U. G. Kyle, I. Bosaeus, A. D. De Lorenzo et al., "Bioelectrical impedance analysis-part I: review of principles and methods," *Clinical Nutrition*, vol. 23, no. 5, pp. 1430–1443, 2004.

[10] U. G. Kyle, I. Bosaeus, A. D. De Lorenzo et al., "Bioelectrical impedance analysis—part II: utilization in clinical practice," *Clinical Nutrition*, vol. 23, no. 6, pp. 1430–1453, 2004.

[11] R. F. Kushner, "Bioelectrical impedance analysis: a review of principles and applications," *Journal of the American College of Nutrition*, vol. 11, no. 2, pp. 199–209, 1992.

[12] G. Parrinello, S. Paterna, P. Di Pasquale et al., "The usefulness of bioelectrical impedance analysis in differentiating dyspnea due to decompensated heart failure," *Journal of Cardiac Failure*, vol. 14, no. 8, pp. 676–686, 2008.

[13] A. P. Hills and N. M. Byrne, "Bioelectrical impedance and body composition assessment," *Malaysian Journal of Nutrition*, vol. 4, pp. 107–112, 1998.

[14] H.-Y. Hu and Y. Kato, "Body composition assessed by bioelectrical impedance analysis (BIA) in patients with Graves'disease before and after treatment," *Endocrine Journal*, vol. 42, no. 4, pp. 545–550, 1995.

[15] R. C. Janaway, S. L. Percival, and A. S. Wilson, "Decomposition of human remains," in *Microbiology and Aging: Clinical Manifestations*, L. Steven Percival, Ed., chapter 13, pp. 313–334, Springer, 2009.

[16] D. Bracco, D. Thiébaud, R. L. Chioléro, M. Landry, P. Burckhardt, and Y. Schutz, "Segmental body composition assessed by bioelectrical impedance analysis and DEXA in humans," *Journal of Applied Physiology*, vol. 81, no. 6, pp. 2580–2587, 1996.

[17] J. M. Jakicic, R. R. Wing, and W. Lang, "Bioelectrical impedance analysis to assess body composition in obese adult women: the effect of ethnicity," *International Journal of Obesity*, vol. 22, no. 3, pp. 243–249, 1998.

[18] L. C. Danford, D. A. Schoeller, and R. F. Kushner, "Comparison of two bioelectrical impedance analysis models for total body water measurement in children," *Annals of Human Biology*, vol. 19, no. 6, pp. 603–607, 1992.

[19] A. Bosy-Westphal, B. Schautz, W. Later, J. J. Kehayias, D. Gallagher, and M. J. Müller, "What makes a BIA equation unique? Validity of eight-electrode multifrequency BIA to estimate body composition in a healthy adult population," *European Journal of Clinical Nutrition*, vol. 67, supplement 1, pp. S14–S21, 2013.

[20] D. A. Schoeller, "Bioelectrical impedance analysis. What does it measure?" *Annals of the New York Academy of Sciences*, vol. 904, pp. 159–162, 2000.

[21] W. J. Rutherford, "Comparison of bioelectrical impedance and skinfolds with hydrodensitometry in the assessment of body composition in healthy young adults," *Journal of Research*, vol. 6, no. 2, pp. 56–60, 2011.

[22] M. E. Orazem and B. Tribollet, *Impedance Spectroscopy*, The ECS Series of Texts and Monographs, Wiley-Inter Sc, 2008.

[23] J. R. Macdonald, "Impedance spectroscopy," *Annals of Biomedical Engineering*, vol. 20, no. 3, pp. 289–305, 1992.

[24] T. Houssin, J. Follet, A. Follet, E. Dei-Cas, and V. Senez, "Label-free analysis of water-polluting parasite by electrochemical impedance spectroscopy," *Biosensors and Bioelectronics*, vol. 25, no. 5, pp. 1122–1129, 2010.

[25] D. A. Scrymgeour, C. Highstrete, Y.-J. Lee, J. W.-P. Hsu, and M. Lee, "High frequency impedance spectroscopy on ZnO nanorod arrays," *Journal of Applied Physics*, vol. 107, no. 6, Article ID 064312, 2010.

[26] J. Nielsen and T. Jacobsen, "Current distribution effects in AC impedance spectroscopy of electroceramic point contact and thin film model electrodes," *Electrochimica Acta*, vol. 55, no. 21, pp. 6248–6254, 2010.

[27] J. Wu, Y. Ben, and H.-C. Chang, "Particle detection by electrical impedance spectroscopy with asymmetric-polarization AC electroosmotic trapping," *Microfluidics and Nanofluidics*, vol. 1, no. 2, pp. 161–167, 2005.

[28] H. E. Ayliffe, A. B. Frazier, and R. D. Rabbitt, "Electric impedance spectroscopy using microchannels with integrated metal electrodes," *Journal of Microelectromechanical Systems*, vol. 8, no. 1, pp. 50–57, 1999.

[29] J. M. Torrents, P. Juan-García, and A. Aguado, "Electrical impedance spectroscopy as a technique for the surveillance of civil engineering structures: considerations on the galvanic insulation of samples," *Measurement Science and Technology*, vol. 18, no. 7, pp. 1958–1962, 2007.

[30] T. Repo, D. H. Paine, and A. G. Taylor, "Electrical impedance spectroscopy in relation to seed viability and moisture content in snap bean (*Phaseolus vulgaris* L.)," *Seed Science Research*, vol. 12, no. 1, pp. 17–29, 2002.

[31] T. Repo, J. Laukkanen, and R. Silvennoinen, "Measurement of the tree root growth using electrical impedance spectroscopy," *Silva Fennica*, vol. 39, no. 2, pp. 159–166, 2005.

[32] E. Barsoukov and J. R. Macdonald, *Impedance Spectroscopy: Theory, Experiment, and Applications*, Wiley-Interscience, 2 edition, 2005.

[33] R. V. Hill, J. C. Jansen, and J. L. Fling, "Electrical impedance plethysmography: a critical analysis," *Journal of Applied Physiology*, vol. 22, no. 1, pp. 161–168, 1967.

[34] J. Nyboer, "Electrical impedance plethysmography; a physical and physiologic approach to peripheral vascular study," *Circulation*, vol. 2, no. 6, pp. 811–821, 1950.

[35] R. W. Griffiths, M. E. Philpot, B. J. Chapman, and K. A. Munday, "Impedance cardiography: non-invasive cardiac output measurement after burn injury," *International Journal of Tissue Reactions*, vol. 3, no. 1, pp. 47–55, 1981.

[36] C. J. Schuster and H. P. Schuster, "Application of impedance cardiography in critical care medicine," *Resuscitation*, vol. 11, no. 3-4, pp. 255–274, 1984.

[37] H. H. Woltjer, H. J. Bogaard, and P. M. J. M. de Vries, "The technique of impedance cardiography," *European Heart Journal*, vol. 18, no. 9, pp. 1396–1403, 1997.

[38] J. G. Webster, *Electrical Impedance Tomography*, Adam Hilger Series of Biomedical Engineering, Adam Hilger, New York, NY, USA, 1st edition, 1990.

[39] D. S. Holder, *Electrical Impedance Tomography: Methods, History and Applications*, Medical Physics and Biomedical Engineering, Institute of Physics Publishing Ltd, 1st edition, 2004.

[40] H. P. Schwan, "Electrical properties of tissue and cell suspensions," *Advances in Biological and Medical Physics*, vol. 5, pp. 147–209, 1957.

[41] G. Ø. Martinsen, S. Grimnes, and H. P. Schwan, "Interface phenomena and dielectric properties of biological tissue," *Encyclopedia of Surface and Colloid Science*, vol. 20, pp. 2643–2653, 2002.

[42] D. Miklavcic, N. Pavselj, and F. X. Hart, *Electric Properties of Tissues*, Wiley Encyclopedia of Biomedical Engineering, John Wiley & Sons, 2006.

[43] Internet Article, JAWON Medical, South Korea, http://www.jawon.co.kr/eng/technology/body-composition/principles-of-bia.php.

[44] T. G. Lohman, *Advances in Body Compositions*, Human Kinetics, Champaign, Ill, USA, 1992.

[45] Internet Article, Bodystat Limited, USA, http://www.bodystat.com/science/.

[46] K. T. Francis, "Body-composition assessment using underwater weighing techniques," *Physical Therapy*, vol. 70, no. 10, pp. 657–663, 1990.

[47] M. K. Oates, "The Use of DXA for Total Body Composition Analysis – Part I, International Society for Clinical Densitometry," SCAN Newsletter, vol. 13, Quarter 2, 6-7.

[48] L. B. Houtkooper, T. G. Lohman, S. B. Going, and W. H. Howell, "Why bioelectrical impedance analysis should be used for estimating adiposity," *American Journal of Clinical Nutrition*, vol. 64, no. 3, supplement, pp. 436S–448S, 1996.

[49] "Internet Article," The Body, Remedy Health Media, New York, USA, http://www.thebody.com/content/art14236.html.

[50] Internet Article and Doylestown Hospital, Pennsylvania 18901, USA, http://www.dh.org/body.cfm?id=1023.

[51] D. N. Lobo, Z. Stanga, J. A. D. Simpson, J. A. Anderson, B. J. Rowlands, and S. P. Allison, "Dilution and redistribution effects of rapid 2-litre infusions of 0.9% (w/v) saline and 5% (w/v) dextrose on haematological parameters and serum biochemistry in normal subjects: a double-blind crossover study," *Clinical Science*, vol. 101, no. 2, pp. 173–179, 2001.

[52] E. Barsoukov and J. R. Macdonald, *Impedance Spectroscopy: Theory, Experiment, and Applications*, Wiley-Interscience, 2005.

[53] J. R. Macdonald, "Impedance spectroscopy," *Annals of Biomedical Engineering*, vol. 20, no. 3, pp. 289–305, 1992.

[54] E. Mark Orazem, *Bernard Tribollet, Electrochemical Impedance Spectroscopy*, The ECS Series of Texts and Monographs, Wiley-Interscience, 1 edition, 2008.

[55] T. K. Bera, Y. Mohamadou, K. H. Lee et al., "Electrical impedance spectroscopy for electro-mechanical characterization of conductive fabrics," *Sensors*, vol. 14, no. 6, pp. 9738–9754, 2014.

[56] A. Lasia, "Electrochemical impedance spectroscopy and its applications," in *Modern Aspects of Electrochemistry*, B. E. Conway, J. Bockris, and R. E. White, Eds., vol. 32, pp. 143–248, Kluwer Academic/Plenum Publishers, New York, NY, USA, 1999.

[57] B.-Y. Chang and S.-M. Park, "Electrochemical impedance spectroscopy," *Annual Review of Analytical Chemistry*, vol. 3, no. 1, pp. 207–229, 2010.

[58] H. Shih and T.-C. Lo, "Electrochemical impedance spectroscopy for battery research and development," Tech. Rep. 31, Solartron Instruments, USA.

[59] A. Ehsani, M. G. Mahjani, and M. Jafarian, "Electrochemical impedance spectroscopy study on intercalation and anomalous diffusion of AlCl-4 ions into graphite in basic molten salt," *Turkish Journal of Chemistry*, vol. 35, no. 5, pp. 735–743, 2011.

[60] J. L. Jespersen, A. E. Tønnesen, K. Nørregaard, L. Overgaard, and F. Elefsen, "Capacity measurements of li-Ion batteries using AC impedance spectroscopy," *World Electric Vehicle Journal*, vol. 3, 2009.

[61] M. Nahvi and B. S. Hoyle, "Electrical impedance spectroscopy sensing for industrial processes," *IEEE Sensors Journal*, vol. 9, no. 12, pp. 1808–1816, 2009.

[62] D. Loveday, P. Peterson, and B. Rodgers, "Evaluation of organic coatings with electrochemical impedance spectroscopy," *JCT CoatingsTech*, vol. 2, no. 2, pp. 22–27, 2005.

[63] M. Ates and A. S. Sarac, "Electrochemical impedance spectroscopy of poly[carbazole-co-N-p-tolylsulfonyl pyrrole] on carbon fiber microelectrodes, equivalent circuits for modelling," *Progress in Organic Coatings*, vol. 65, no. 2, pp. 281–287, 2009.

[64] J. Yu and C.-C. Liu, "Microfabricated thin film impedance sensor & AC impedance measurements," *Sensors*, vol. 10, no. 6, pp. 5845–5858, 2010.

[65] M. Metikoš-Huković and S. Omanović, "Thin indium oxide film formation and growth: impedance spectroscopy and cyclic voltammetry investigations," *Journal of Electroanalytical Chemistry*, vol. 455, no. 1-2, pp. 181–189, 1998.

[66] M.-G. Olivier and M. Poelman, "Use of electrochemical impedance spectroscopy (EIS) for the evaluation of electrocoatings performances, recent researches," in *Corrosion Evaluation and Protection*, R. S. Razavi, Ed., InTech, 2012.

[67] F. Kurniawan, *New analytical applications of gold nanoparticles [Ph.D. thesis]*, University of Regensburg, Regensburg, Germany, 2008.

[68] J. P. Lynch, K. J. Loh, and N. Kotov, "Electrical impedance analysis of carbon nanotube-polyelectrolyte thin film strain sensors," in *Proceedings of the US-Korea Workshop on Smart Structures Technology for Steel Structures*, Seoul, Korea, 2006.

[69] A. S. Sarac, M. Ates, and B. Kilic, "Electrochemical impedance spectroscopic study of polyaniline on platinum, glassy carbon and carbon fiber microelectrodes," *International Journal of Electrochemical Science*, vol. 3, pp. 777–786, 2008.

[70] W. Yang, J. E. Butler, J. N. Russell Jr., and R. J. Hamers, "Direct electrical detection of antigen-antibody binding on diamond and silicon substrates using electrical impedance spectroscopy," *Analyst*, vol. 132, no. 4, pp. 296–306, 2007.

[71] A. Vandenberg and K. J. Loh, "Evaluating the Ph sensitivity of carbon nanotube-polyaniline thin films with different dopants," *Nano LIFE*, vol. 2, no. 4, Article ID 1242001, 12 pages, 2012.

[72] D. A. Dean, T. Ramanathan, D. Machado, and R. Sundararajan, "Electrical impedance spectroscopy study of biological tissues," *Journal of Electrostatics*, vol. 66, no. 3-4, pp. 165–177, 2008.

[73] P. Heroux and M. Bourdages, "Monitoring living tissues by electrical impedance spectroscopy," *Annals of Biomedical Engineering*, vol. 22, no. 3, pp. 328–337, 1994.

[74] J. Estrela da Silva, J. P. Marques de Sá, and J. Jossinet, "Classification of breast tissue by electrical impedance spectroscopy," *Medical and Biological Engineering and Computing*, vol. 38, no. 1, pp. 26–30, 2000.

[75] C. Skourou, P. J. Hoopes, R. R. Strawbridge, and K. D. Paulsen, "Feasibility studies of electrical impedance spectroscopy for early tumor detection in rats," *Physiological Measurement*, vol. 25, no. 1, pp. 335–346, 2004.

[76] T. K. Bera, J. K. Seo, H. Kwon, and J. Nagaraju, "A LabVIEW based electrical bio-impedance spectroscopic data interpreter (LEBISDI) for studying the equivalent circuit parameters of biological tissues," in *Proceedings of the 15th International Conference on Electrical Bio-Impedance (ICEBI) and 14th Conference on Electrical Impedance Tomography (EIT)*, p. 77, Berlin, Germany, April 2013.

[77] J. M. Cruza, I. C. Fitaa, L. Sorianob, J. Payáb, and M. V. Borracherob, "The use of electrical impedance spectroscopy for monitoring the hydration products of Portland cement mortars with high percentage of pozzolans," *Cement and Concrete Research*, vol. 50, pp. 51–61, 2013.

[78] L. Dhouibi, E. Triki, and A. Raharinaivo, "The application of electrochemical impedance spectroscopy to determine the long-term effectiveness of corrosion inhibitors for steel in concrete," *Cement and Concrete Composites*, vol. 24, no. 1, pp. 35–43, 2002.

[79] A. Akhavan and F. Rajabipour, "Evaluating ion diffusivity of cracked cement paste using electrical impedance spectroscopy," *Materials and Structures*, vol. 46, no. 5, pp. 697–708, 2013.

[80] M. Tiitta and H. Olkkonen, "Electrical impedance spectroscopy device for measurement of moisture gradients in wood," *Review of Scientific Instruments*, vol. 73, no. 8, p. 3093, 2002.

[81] M. Tiitta, T. Savolainen, H. Olkkonen, and T. Kanko, "Wood moisture gradient analysis by electrical impedance spectroscopy," *Holzforschung*, vol. 53, no. 1, pp. 68–76, 1999.

[82] S. L. Zelinka, D. R. Rammer, and D. S. Stone, "Impedance spectroscopy and circuit modeling of Southern pine above 20% moisture content," *Holzforschung*, vol. 62, no. 6, pp. 737–744, 2008.

[83] X. Liu, *Electrical impedance spectroscopy applied in plant physiology studies [M.S. thesis]*, RMIT University, Melbourne, Australia, 2006.

[84] A. Hakam, M. M. Takam, M. Chokairi et al., "Effect of bark stripping on the electrical impedance of quercus suber leaves, maderas," *Ciencia y Tecnología*, vol. 14, no. 2, pp. 195–208, 2012.

[85] S. Ha, M. Diez-Silva, E. Du et al., "Microfluidic electric impedance spectroscopy for Malaria diagnosis," in *Proceedings of the 16th International Conference on Miniaturized Systems for Chemistry and Life Sciences*, pp. 1960–1962, Okinawa, Japan, 2012.

[86] S. Ha, *A malaria diagnostic system based on electric impedance spectroscopy [M.S. thesis]*, Massachusetts Institute of Technology, Boston, Mass, USA, 2011.

[87] J. Wu, Y. Ben, and H.-C. Chang, "Particle detection by electrical impedance spectroscopy with asymmetric-polarization AC electroosmotic trapping," *Microfluidics and Nanofluidics*, vol. 1, no. 2, pp. 161–167, 2005.

[88] A. Fattah-alhosseini, S. Taheri Shoja, B. Heydari Zebardast, and P. Mohamadian Samim, "An electrochemical impedance

spectroscopic study of the passive state on AISI 304 stainless steel," *International Journal of Electrochemistry*, vol. 2011, Article ID 152143, 8 pages, 2011.

[89] A. M. A. Alsamuraee, H. I. Jaafer, H. A. Ameen, and A. Q. Abdullah, "Electrochemical impedance spectroscopic evaluation of corrosion protection properties of polyurethane/polyvinyl chloride blend coatings on steel," *American Journal of Scientific and Industrial Research*, vol. 2, no. 5, pp. 761–768, 2011.

[90] T. K. Bera and J. Nagaraju, "Electrical impedance spectroscopic studies of the electronic connectors of DIP switch based multiplexers suitable for multifrequency electrical impedance tomography, biomedical engineering, Narosa Publishing House," in *Proceeding of the International Conference on Biomedical Engineering (ICBME '11)*, pp. 58–65, Manipal, India, 2011.

[91] P. M. Gomadam and J. W. Weidner, "Analysis of electrochemical impedance spectroscopy in proton exchange membrane fuel cells," *International Journal of Energy Research*, vol. 29, no. 12, pp. 1133–1151, 2005.

[92] J. Yu and C.-C. Liu, "Microfabricated thin film impedance sensor & AC impedance measurements," *Sensors*, vol. 10, no. 6, pp. 5845–5858, 2010.

[93] T. Ryll, A. Brunner, S. Ellenbroek, A. Bieberle-Hutter, J. L. M. Rupp, and L. J. Gauckler, "Electrical conductivity and crystallization of amorphous bismuth ruthenate thin films deposited by spray pyrolysis," *Physical Chemistry Chemical Physics*, vol. 12, no. 42, pp. 13933–13942, 2010.

[94] J. Nyboer, "Plethysmography. Impedance," in *Medical Physics*, O. Glasser, Ed., vol. 2, pp. 736–743, Year Book, Chicago, Ill, USA, 1950.

[95] J. Nyboer, S. Bango, and L. F. Nims, "The impedance plethysmograph and electrical volume recorder," CAM Report 149, OSPR, 1943.

[96] D. K. Swanson and J. G. Webster, "Origin of the electrical impedance pulse in the limbs," in *Proceedings of the 29th Annual Conference on Engineering in Medicine & Biology*, vol. 18, p. 324, 1976.

[97] J. G. Webster, *Medical Instrumentation Application and Design*, Wiley, 4 edition, 2009.

[98] D. Wade Peterson, "Internet Article, Phoenix Ambulatory Blood Pressure Monitor Project, Sub-project: Impedance Plethysmograph Sensor," http://www.thebody.com/content/art14236.html.

[99] Internet Article, http://www.sti.nasa.gov/tto/spinoff2001/hm1.html.

[100] J. Malmivuo and R. Plonsey, *Bioelectromagnetism: Principles and Applications of Bioelectric and Biomagnetic Fields*, Oxford University Press, New York, NY, USA, 1995.

[101] Internet Article, "Overview of Impedance Cardiography (ICG)," http://impedancecardiography.com/icgover10.html.

[102] M. H. F. Ribeiro, R. W. dos Santos, L. Paulo, S. Barra, and F. C. Peters, "Simulation study on the determination of cardiac ejection fraction by electrical impedance tomography using a hybrid heuristic approach," *Journal of Medical Imaging and Health Informatics*, vol. 4, pp. 113–121, 2014.

[103] T. K. Bera, "Noninvasive electromagnetic methods for brain monitoring: a technical review," in *Brain Computer Interfaces: Current Trends and Applications*, Intelligent Systems Reference Library, Chapter 2, Springer, 2014.

[104] T. K. Bera and J. Nagaraju, "Electrical Impedance Tomography (EIT): a harmless medical imaging modality," in *Research Developments in Computer Vision and Image Processing: Methodologies and Applications*, chapter 13, pp. 224–262, IGI Global USA.

[105] J. K. Seo and E. J. Woo, *Nonlinear Inverse Problems in Imaging*, Wiley, 1 edition, December 2012.

[106] T. K. Bera and J. Nagaraju, "Sensors for electrical impedance tomography," in *The Measurement, Instrumentation, and Sensors Handbook*, J. G. Webster, Ed., chapter 61, pp. 61.1–61.30, CRC Press, 2nd edition, 2014.

[107] P. Metherall, *Three dimensional electrical impedance tomography of the human thorax [Ph.D. thesis]*, University of Sheffield, 1998.

[108] T. K. Bera, *Studies on multi frequency Electrical Impedance Tomography (EIT) to improve the impedance imaging for biomedical applications [Ph.D. thesis]*, Department of Instrumentation and Applied Physics, Indian Institute of Science, Bangalore, India.

[109] P. Metherall, D. C. Barber, R. H. Smallwood, and B. H. Brown, "Three-dimensional electrical impedance tomography," *Nature*, vol. 380, no. 6574, pp. 509–512, 1996.

[110] T. K. Bera and J. Nagaraju, "Studies on thin film based flexible gold electrode arrays for resistivity imaging in electrical impedance tomography," *Measurement*, vol. 47, pp. 264–286, 2014.

[111] L. Borcea, "Electrical impedance tomography," *Inverse Problems*, vol. 18, no. 6, pp. R99–R136, 2002.

[112] B. H. Brown, "Electrical impedance tomography (EIT): a review," *Journal of Medical Engineering and Technology*, vol. 27, no. 3, pp. 97–108, 2003.

[113] R. H. Bayford, "Bioimpedance tomography (electrical impedance tomography)," *Annual Review of Biomedical Engineering*, vol. 8, pp. 63–91, 2006.

[114] E. L. Costa, R. G. Lima, and M. B. Amato, "Electrical impedance tomography," *Current Opinion in Critical Care*, vol. 15, no. 1, pp. 18–24, 2009.

[115] T. K. Bera and N. Jampana, "A Multifrequency constant current source for medical electrical impedance tomography," in *Proceedings of the IEEE International Conference on Systems in Medicine and Biology*, pp. 290–295, Kharagpur, India, December 2010.

[116] T. I. Oh, H. Koo, K. H. Lee et al., "Validation of a multifrequency electrical impedance tomography (mfEIT) system KHU Mark1: impedance spectroscopy and time-difference imaging," *Physiological Measurement*, vol. 29, no. 3, pp. 295–307, 2008.

[117] T. K. Bera and J. Nagaraju, "A study of practical biological phantoms with simple instrumentation for Electrical Impedance Tomography (EIT)," in *Proceedings of the IEEE Intrumentation and Measurement Technology Conference (I2MTC '09)*, pp. 511–516, Singapore, May 2009.

[118] P. J. Riu, J. Rosell, A. Lozano, and R. Pallas-Areny, "Multifrequency static imaging in electrical impedance tomography: part 1 instrumentation requirements," *Medical and Biological Engineering and Computing*, vol. 33, no. 6, pp. 784–792, 1995.

[119] T. K. Bera, M. Saikia, and J. Nagaraju, "A Battery-based Constant Current Source (Bb-CCS) for Biomedical Applications," in *International Conference on Computing, Communication and Networking Technologies (ICCCNT '13)*, Tamilnadu, India, 2013.

[120] T. I. Oh, H. Wi, D. Y. Kim, P. J. Yoo, and E. J. Woo, "A fully parallel multi-frequency EIT system with flexible electrode configuration: KHU Mark2," *Physiological Measurement*, vol. 32, no. 7, pp. 835–849, 2011.

[121] T. K. Bera and J. Nagaraju, "A LabVIEW based multifunction multifrequency electrical impedance tomography (MfMf-EIT) instrumentation for flexible and versatile impedance imaging," in *Proceedings of the 15th International Conference on Electrical Bio-Impedance (ICEBI '13) and 14th Conference on Electrical Impedance Tomography (EIT '13)*, p. 216, Berlin, Germany, 2013.

[122] K. G. Boone and D. S. Holder, "Current approaches to analogue instrumentation design in electrical impedance tomography," *Physiological Measurement*, vol. 17, no. 4, pp. 229–247, 1996.

[123] T. K. Bera and J. Nagaraju, "A Battery Based Multifrequency Electrical Impedance Tomography (BbMf-EIT) system for impedance, imaging of human anatomy," in *Proceedings of the 15th International Conference on Electrical Bio-Impedance (ICEBI) and 14th Conference on Electrical Impedance Tomography (EIT' 13)*, p. 217, Berlin, Germany, 2013.

[124] W. R. B. Lionheart, "EIT reconstruction algorithms: pitfalls, challenges and recent developments," *Physiological Measurement*, vol. 25, no. 1, pp. 125–142, 2004.

[125] S. Teniou and M. Meribout, "A new hierarchical reconstruction algorithm for electrical capacitance tomography using a relaxation region-based approach," *Measurement*, vol. 45, no. 4, pp. 683–690, 2012.

[126] L.-M. Wang, Y.-L. Zhao, F.-L. Chen, and Y. Han, "The 3D CT reconstruction algorithm to directly reconstruct multicharacteristic based on EMD," *Measurement*, vol. 44, no. 10, pp. 2043–2048, 2011.

[127] S.-W. Chen and C.-Y. Chu, "A comparison of 3D cone-beam Computed Tomography (CT) image reconstruction performance on homogeneous multi-core processor and on other processors," *Measurement*, vol. 44, no. 10, pp. 2035–2042, 2011.

[128] T. K. Bera, S. K. Biswas, K. Rajan, and J. Nagaraju, "Improving image quality in Electrical Impedance Tomography (EIT) using Projection Error Propagation-Based Regularization (PEPR) technique: a simulation study," *Journal of Electrical Bioimpedance*, vol. 2, pp. 2–12, 2011.

[129] T. K. Bera, S. K. Biswas, K. Rajan, and J. Nagaraju, "Image reconstruction in Electrical Impedance Tomography (EIT) with projection error propagation-based regularization (PEPR): a practical phantom study," in *Advanced Computing, Networking and Security*, vol. 7135 of *Lecture Notes in Computer Science*, Springer, 2012.

[130] T. K. Bera, S. K. Biswas, K. Rajan, and J. Nagaraju, "Improving conductivity image quality using Block Matrix-based Multiple Regularization (BMMR) technique in EIT: a simulation study," *Journal of Electrical Bioimpedance*, vol. 2, pp. 33–47, 2011.

[131] T. K. Bera, S. K. Biswas, K. Rajan, and N. Jampana, "Improving the image reconstruction in Electrical Impedance Tomography (EIT) with block matrix-based Multiple Regularization (BMMR): a practical phantom study," in *Proceedings of the World Congress on Information and Communication Technologies (WICT '11)*, pp. 1346–1351, University of Mumbai, Mumbai, India, December 2011.

[132] F. Yang, J. Zhang, and R. Patterson, "Development of an anatomically realistic forward solver for thoracic electrical impedance tomography," *Journal of Medical Engineering*, vol. 2013, Article ID 983938, 7 pages, 2013.

[133] L. Jing, S. Liu, L. Zhihong, and S. Meng, "An image reconstruction algorithm based on the extended Tikhonov regularization method for electrical capacitance tomography," *Measurement*, vol. 42, no. 3, pp. 368–376, 2009.

[134] J. Davis and P. Wells, "Computed tomographymeasurements on wood," *Industrial Metrology*, vol. 2, no. 3-4, pp. 195–218, 1992.

[135] J. Hiller and L. M. Reindl, "A computer simulation platform for the estimation of measurement uncertainties in dimensional X-ray computed tomography," *Measurement*, vol. 45, no. 8, pp. 2166–2182, 2012.

[136] G. Andria, F. Attivissimo, and A. M. L. Lanzolla, "A statistical approach for MR and CT images comparison," *Measurement*, vol. 46, pp. 57–65, 2013.

[137] X. Zhang, N. Homma, S. Goto et al., "A hybrid image filtering method for computer-aided detection of microcalcification clusters in mammograms," *Journal of Medical Engineering*, vol. 2013, Article ID 615254, 8 pages, 2013.

[138] G. Betta, D. Capriglione, and N. Pasquino, "Experimental investigation on workers'exposure to electromagnetic fields in proximity of magnetic resonance imaging systems," *Measurement*, vol. 45, no. 2, pp. 199–206, 2012.

[139] B. Leporq, S. Camarasu-Pop, E. E. Davila-Serrano, F. Pilleul, and O. Beuf, "Enabling 3D-liver perfusion mapping from MR-DCE imaging using distributed computing," *Journal of Medical Engineering*, vol. 2013, Article ID 471682, 7 pages, 2013.

[140] M. Almoudi and Z. Sun, "Myocardial perfusion imaging using ^{99}mTc-MIBI single photon emission computed tomography: a cardiac phantom study," *Journal of Medical Imaging and Health Informatics*, vol. 3, pp. 480–486, 2013.

[141] C. Imperiale and A. Imperiale, "Some fast calculations simulating measurements from single-photon emission computed tomography (SPECT) imaging," *Measurement*, vol. 37, no. 3, pp. 218–240, 2005.

[142] L. García-Rojas Adame-Ocampo, G. Mendoza-Vázquez, E. Alexánderson, and J. L. Tovilla-Canales, "Orbital positron emission tomography/computed tomography (PET/CT) imaging findings in graves ophthalmopathy," *BMC Research Notes*, vol. 6, p. 353, 2013.

[143] C. A. Yi, K. S. Lee, H. Y. Lee et al., "Coregistered whole body magnetic resonance imaging-positron emission tomography (MRI-PET) versus PET-computed tomography plus brain MRI in staging resectable lung cancer: comparisons of clinical effectiveness in a randomized trial," *Cancer*, vol. 119, no. 10, pp. 1784–1791, 2013.

[144] A. Fenster, K. Surry, W. Smith, and D. B. Downey, "The use of three-dimensional ultrasound imaging in breast biopsy and prostate therapy," *Measurement*, vol. 36, no. 3-4, pp. 245–256, 2004.

[145] G. Andria, F. Attivissimo, G. Cavone, N. Giaquinto, and A. M. L. Lanzolla, "Linear filtering of 2-D wavelet coefficients for denoising ultrasound medical images," *Measurement*, vol. 45, no. 7, pp. 1792–1800, 2012.

[146] D. S. Holder, *Clinical and Physiological Applications of Electrical Impedance Tomography*, Taylor & Francis, UCL Press, UCL, London, UK, 1st edition, 1993.

[147] Y. Li, L. Rao, R. He et al., "A novel combination method of electrical impedance tomography inverse problem for brain imaging," *IEEE Transactions on Magnetics*, vol. 41, no. 5, pp. 1848–1851, 2005.

[148] D. Murphy, P. Burton, R. Coombs, L. Tarassenko, and P. Rolfe, "Impedance imaging in the newborn," *Clinical Physics and Physiological Measurement*, vol. 8, no. 4, supplement, pp. 131–140, 1987.

[149] H. A. Tyna and S. E. Iles, "Technology review: the use of electrical impedance scanning in the detection of breast cancer," *Breast Cancer Research*, vol. 6, no. 2, pp. 69–74, 2004.

[150] F. S. Moura, J. C. C. Aya, A. T. Fleury, M. B. P. Amato, and R. G. Lima, "Dynamic imaging in electrical impedance tomography

of the human chest with online transition matrix identification," *IEEE Transactions on Bio-Medical Engineering*, vol. 57, no. 2, pp. 422–431, 2010.

[151] F. Ferraioli, A. Formisano, and R. Martone, "Effective exploitation of prior information in electrical impedance tomography for thermal monitoring of hyperthermia treatments," *IEEE Transactions on Magnetics*, vol. 45, no. 3, pp. 1554–1557, 2009.

[152] W. He, P. Ran, Z. Xu, B. Li, and S.-N. Li, "A 3D visualization method for bladder filling examination based on EIT, computational and mathematical methods in medicine," vol. 2012, Article ID 528096, 9 pages, 2012.

[153] J. L. Davidson, L. S. Ruffino, D. R. Stephenson, R. Mann, B. D. Grieve, and T. A. York, "Three-dimensional electrical impedance tomography applied to a metal-walled filtration test platform," *Measurement Science and Technology*, vol. 15, no. 11, pp. 2263–2274, 2004.

[154] G. T. Bolton, C. H. Qiu, and M. Wang, "A novel electrical tomography sensor for monitoring the phase distribution in industrial reactors," in *Proceedings of the 7th UK Conference-Fluid Mixing*, Bradford, UK, July 2002.

[155] F. Dickin and M. Wang, "Electrical resistance tomography for process applications," *Measurement Science and Technology*, vol. 7, no. 3, pp. 247–260, 1996.

[156] T.-C. Hou, K. J. Loh, and J. P. Lynch, "Spatial conductivity mapping of carbon nanotube composite thin films by electrical impedance tomography for sensing applications," *Nanotechnology*, vol. 18, no. 31, Article ID 315501, 2007.

[157] T. Sun, S. Tsuda, K.-P. Zauner, and H. Morgan, "On-chip electrical impedance tomography for imaging biological cells," *Biosensors and Bioelectronics*, vol. 25, no. 5, pp. 1109–1115, 2010.

[158] P. Linderholm, L. Marescot, M. H. Loke, and P. Renaud, "Cell culture imaging using microimpedance tomography," *IEEE Transactions on Biomedical Engineering*, vol. 55, no. 1, pp. 138–146, 2008.

[159] F. Djamdji, A. C. Gorvin, I. L. Freeston, R. C. Tozer, I. C. Mayes, and S. R. Blight, "Electrical impedance tomography applied to semiconductor wafer characterization," *Measurement Science and Technology*, vol. 7, no. 3, pp. 391–395, 1996.

[160] K. Karhunen, A. Seppänen, A. Lehikoinen, P. J. M. Monteiro, and J. P. Kaipio, "Electrical Resistance Tomography imaging of concrete," *Cement and Concrete Research*, vol. 40, no. 1, pp. 137–145, 2010.

[161] J. E. Chambers, P. B. Wilkinson, D. Wardrop et al., "Bedrock detection beneath river terrace deposits using three-dimensional electrical resistivity tomography," *Geomorphology*, vol. 177-178, pp. 17–25, 2012.

[162] P. Church, J. E. McFee, S. Gagnon, and P. Wort, "Electrical impedance tomographic imaging of buried landmines," *IEEE Transactions on Geoscience and Remote Sensing*, vol. 44, no. 9, pp. 2407–2420, 2006.

[163] B. Ullrich, T. Günther, and C. Rücker, "Electrical resistivity tomography methods for archaeological prospection," in *Proceedings of the 35th International Conference on Computer Applications and Quantitative Methods in Archaeology (CAA '07)*, A. Posluschny, K. Lambers, and I. Herzog, Eds., pp. 1–7, Berlin, Germany, 2007, Koll. Vor- u. Frühgesch. 10 (Bonn 2008).

[164] M. Ingham, D. Pringle, and H. Eicken, "Cross-borehole resistivity tomography of sea ice," *Cold Regions Science and Technology*, vol. 52, no. 3, pp. 263–277, 2008.

[165] G. D'Antona and L. Rocca, "Electrical impedance tomography for underground pollutant detection and polluted lands reclaiming monitoring," in *Proceedings of the 19th IEEE Intrumentation and Measurement Technology Conference*, pp. 1035–1038, Anchorage, Alaska, USA, May 2002.

[166] A. Yao, C. L. Yang, J. K. Seo, and M. Soleimani, "EIT-based fabric pressure sensing, computational and mathematical methods in medicine," *Computational and Mathematical Methods in Medicine*, vol. 2013, Article ID 405325, 9 pages, 2013.

[167] H. Gao, C. Xu, F. Fu, and S. Wang, "Effects of particle charging on electrical capacitance tomography system," *Measurement*, vol. 45, no. 3, pp. 375–383, 2012.

[168] Z. Fan, R. X. Gao, and J. Wang, "Virtual instrument for online electrical capacitance tomography," in *Practical Applications and Solutions Using LabVIEW*, F. Silviu, Ed., under CC BY-NC-SA 3.0 license, 2011.

[169] A. Perrone, G. Zeni, S. Piscitelli et al., "Joint analysis of SAR interferometry and electrical resistivity tomography surveys for investigating ground deformation: the case-study of Satriano di Lucania (Potenza, Italy)," *Engineering Geology*, vol. 88, no. 3-4, pp. 260–273, 2006.

[170] A. Finizola, A. Revil, E. Rizzo et al., "Hydrogeological insights at Stromboli volcano (Italy) from geoelectrical, temperature, and CO_2 soil degassing investigations," *Geophysical Research Letters*, vol. 33, no. 17, Article ID L17304, 2006.

[171] A. Beauvais, M. Ritz, J.-C. Parisot, C. Bantsimba, and M. Dukhan, "Combined ERT and GPR methods for investigating two-stepped lateritic weathering systems," *Geoderma*, vol. 119, no. 1-2, pp. 121–132, 2004.

[172] A. Kemna, B. Kulessa, and H. Vereecken, "Imaging and characterisation of subsurface solute transport using electrical resistivity tomography (ERT) and equivalent transport models," *Journal of Hydrology*, vol. 267, no. 3-4, pp. 125–146, 2002.

[173] H. Karabulut, S. Özalaybey, T. Taymaz, M. Aktar, O. Selvi, and A. Kocaoğlu, "A tomographic image of the shallow crustal structure in the Eastern Marmara," *Geophysical Research Letters*, vol. 30, no. 24, pp. 1–10, 2003.

[174] D. C. Barber and B. H. Brown, "Applied potential tomography," *Journal of Physics E*, vol. 17, pp. 723–734, 1984.

[175] J. Kuen, E. J. Woo, and J. K. Seo, "Multi-frequency time-difference complex conductivity imaging of canine and human lungs using the KHU Mark1 EIT system," *Physiological Measurement*, vol. 30, no. 6, pp. S149–S164, 2009.

[176] T. I. Oh, H. Koo, K. H. Lee et al., "Validation of a multi-frequency electrical impedance tomography (mfEIT) system KHU Mark1: impedance spectroscopy and time-difference imaging," *Physiological Measurement*, vol. 29, no. 3, pp. 295–307, 2008.

[177] B. Harrach, J. K. Seo, and E. J. Woo, "Factorization method and its physical justification in frequency-difference electrical impedance tomography," *IEEE Transactions on Medical Imaging*, vol. 29, no. 11, pp. 1918–1926, 2010.

[178] J. K. Seo, J. Lee, S. W. Kim, H. Zribi, and E. J. Woo, "Frequency-difference electrical impedance tomography (fdEIT): algorithm development and feasibility study," *Physiological Measurement*, vol. 29, no. 8, pp. 929–944, 2008.

[179] M. Molinary, *High fidelity imaging in electrical impedance tomography [Ph.D. thesis]*, University of Southampton, Southampton, UK, 2003.

[180] T. K. Bera and J. Nagaraju, "Studying the variations of complex electrical bio-impedance of vegetables and fruits under the different health status," in *Proceedings of the 15th International Conference on Electrical Bio-Impedance (ICEBI '13) and 14th*

Conference on Electrical Impedance Tomography (EIT '13), p. 193, Germany, April 2013.

[181] P. L. M. Cox-Reijven, B. Van Kreel, and P. B. Soeters, "Bioelectrical impedance spectroscopy: alternatives for the conventional hand-to-foot measurements," *Clinical Nutrition*, vol. 21, no. 2, pp. 127–133, 2002.

[182] A. Romsauerova, A. McEwan, L. Horesh, R. Yerworth, R. H. Bayford, and D. S. Holder, "Multi-frequency electrical impedance tomography (EIT) of the adult human head: initial findings in brain tumours, arteriovenous malformations and chronic stroke, development of an analysis method and calibration," *Physiological Measurement*, vol. 27, no. 5, pp. S147–S161, 2006.

[183] N. K. Soni, A. Hartov, C. Kogel, S. P. Poplack, and K. D. Paulsen, "Multi-frequency electrical impedance tomography of the breast: new clinical results," *Physiological Measurement*, vol. 25, no. 1, pp. 301–314, 2004.

[184] H. Wi, T. E. Kim, T. I. Oh, and E. J. Woo, "Expandable multifrequency EIT system for clinical applications," in *Progress In Electromagnetics Research Symposium Proceedings*, pp. 49–52, Kuala Lumpur, Malaysia, 2012.

[185] T. I. Oh, H. Koo, K. H. Lee et al., "Validation of a multifrequency electrical impedance tomography (mfEIT) system KHU Mark1: impedance spectroscopy and time-difference imaging," *Physiological Measurement*, vol. 29, no. 3, pp. 295–307, 2008.

[186] T. K. Bera and J. Nagaraju, "Gold electrode sensors for Electrical Impedance Tomography (EIT) studies," in *IEEE Sensors Application Symposium*, pp. 24–28, San Antonio, Tex, USA, 2011.

[187] T. K. Bera and J. Nagaraju, *Studying the 2D Resistivity Reconstruction of Stainless Steel Electrode Phantoms Using Different Current Patterns of Electrical Impedance Tomography (EIT), Biomedical Engineering*, Narosa Publishing House, 2011.

[188] T. K. Bera and J. Nagaraju, "Studying the resistivity imaging of chicken tissue phantoms with different current patterns in Electrical Impedance Tomography (EIT)," *Measurement*, vol. 45, no. 4, pp. 663–682, 2012.

[189] T. J. Yorkey, *Comparing reconstruction methods for electrical impedance tomography [Ph.D. thesis]*, University of Wisconsin at Madison, Madison, Wis, USA, 1986.

[190] T. J. Yorkey, J. G. Webster, and W. J. Tompkins, "Comparing reconstruction algorithms for electrical impedance tomography," *IEEE Transactions on Biomedical Engineering*, vol. 34, no. 11, pp. 843–852, 1987.

[191] W. R. B. Lionheart, "EIT reconstruction algorithms: pitfalls, challenges and recent developments," *Physiological Measurement*, vol. 25, no. 1, pp. 125–142, 2004.

[192] V. Marko, *Electrical Impedance Tomography and Prior Information*, Kuopio University Publications, Natural and Environmental Sciences, 1997.

[193] C. J. Grootveld, *Measuring and modeling of concentrated settling suspensions using electrical impedance tomography [Ph.D. thesis]*, Delft University of Technology, The Netherlands, 1996.

[194] B. M. Graham, *Enhancements in Electrical Impedance Tomography (EIT) image reconstruction for 3D lung imaging [Ph.D. thesis]*, University of Ottawa, 2007.

[195] T. K. Bera and J. Nagaraju, "A FEM-based forward solver for studying the forward problem of electrical impedance tomography (EIT) with a practical biological phantom," in *Proceedings of the IEEE International Advance Computing Conference (IACC '09)*, pp. 1375–1381, Patiala, India, March 2009.

[196] J. N. Reddy, *Introduction to the Finite Element Method*, TATA McGraw-Hill Publishing Company Ltd., Delhi, India, 3rd edition, 2006.

[197] T. K. Bera and J. Nagaraju, "A gold sensors array for imaging the real tissue phantom in electrical impedance tomography," in *International Conference on Materials Science and Technology*, Kerala, India, 2012.

[198] D. S. Holder, Y. Hanquan, and A. Rao, "Some practical biological phantoms for calibrating multifrequency electrical impedance tomography," *Physiological Measurement*, vol. 17, no. 4, pp. A167–A177, 1996.

[199] T. K. Bera and J. Nagaraju, "A stainless steel electrode phantom to study the forward problem of Electrical Impedance Tomography (EIT)," *Sensors and Transducers Journal*, vol. 104, no. 5, pp. 33–40, 2009.

[200] T. K. Bera and J. Nagaraju, "A chicken tissue phantom for studying an electrical impedance tomography (EIT) system suitable for clinical imaging," *Sensing and Imaging*, vol. 12, no. 3-4, pp. 95–116, 2011.

[201] H. Griffiths, "A phantom for electrical impedance tomography," *Clinical Physics and Physiological Measurement A*, vol. 9, supplement, pp. 15–20, 1988.

[202] M. Sperandio, M. Guermandi, and R. Guerrieri, "A four-shell diffusion phantom of the head for electrical impedance tomography," *IEEE Transactions on Biomedical Engineering*, vol. 59, no. 2, pp. 383–389, 2012.

[203] G. Hahn, M. Beer, I. Frerichs, T. Dudykevych, T. Schröder, and G. Hellige, "A simple method to check the dynamic performance of electrical impedance tomography systems," *Physiological Measurement*, vol. 21, no. 1, pp. 53–60, 2000.

[204] G. Hahn, A. Just, and G. Hellige, "Determination of the dynamic measurement error of EIT systems," in *Proceedings of the 13th International Conference on Electrical Bioimpedance and the 8th Conference on Electrical Impedance Tomography (ICEBI '07)*, pp. 320–323, September 2007.

[205] A. E. Hartinger, H. Gagnon, and R. Guardo, "A method for modelling and optimizing an electrical impedance tomography system," *Physiological Measurement*, vol. 27, no. 5, pp. S51–S64, 2006.

[206] A. E. Hartinger, H. Gagnon, and R. Guardo, "Accounting for hardware imperfections in EIT image reconstruction algorithms," *Physiological Measurement*, vol. 28, no. 7, pp. S13–S27, 2007.

[207] H. Gagnon, A. E. Hartinger, A. Adler, and R. Guardo, "A resistive mesh phantom for assessing the performance of EIT systems," in *EIT Conference*, Manchester, UK, 2009.

[208] G. Hahn, A. Just, J. Dittmar, and G. Hellige, "Systematic errors of EIT systems determined by easily-scalable resistive phantoms," *Physiological Measurement*, vol. 29, pp. S163–S172, 2008.

[209] H. Gagnon, Y. Sigmen, A. E. Hartinger, and R. Guardo, *An Active Phantom to Assess the Robustness of EIT Systems to Electrode Contact Impedance Variations*, EIT, Manchester, UK, 2009.

[210] T. K. Bera and J. Nagaraju, "Resistivity imaging of a reconfigurable phantom with circular inhomogeneities in 2D-electrical impedance tomography," *Measurement*, vol. 44, no. 3, pp. 518–526, 2011.

[211] T. K. Bera and J. Nagaraju, "Common ground method of current injection in electrical impedance tomography," in *Proceedings of the 4th International Conference on Recent trends in Computing, Communication & Information Technologies*, vol. 270, pp. 593–605, Tamil Nadu, India, 2011.

[212] T. K. Bera and J. Nagaraju, "Studying the 2D-image reconstruction of non biological and biological inhomogeneities in Electrical Impedance Tomography (EIT) with EIDORS," in *International Conference on Advanced Computing, Networking and Security*, pp. 132–136, Mangalore, India, 2011.

[213] T. K. Bera, S. K. Biswas, K. Rajan, and N. Jampana, "Improving the image reconstruction in Electrical Impedance Tomography (EIT) with block matrix-based Multiple Regularization (BMMR): a practical phantom study," in *Proceedings of the World Congress on Information and Communication Technologies (WICT '11)*, pp. 1346–1351, Mumbai, India, December 2011.

[214] T. K. Bera, S. K. Biswas, K. Rajan, and J. Nagaraju, "Image reconstruction in Electrical Impedance Tomography (EIT) with projection error propagation-based regularization (PEPR): a practical phantom study," in *Advanced Computing, Networking and Security*, vol. 7135 of *Lecture Notes in Computer Science*, pp. 95–105, 2012.

[215] T. K. Bera and J. Nagaraju, "A multifrequency Electrical Impedance Tomography (EIT) system for biomedical imaging," in *International Conference on Signal Processing and Communications*, pp. 1–5, Bangalore, India, 2012.

[216] N. K. Soni, H. Dehghani, A. Hartov, and K. D. Paulsen, "A novel data calibration scheme for electrical impedance tomography," *Physiological Measurement*, vol. 24, no. 2, pp. 421–435, 2003.

[217] G. Qiao, W. Wang, L. Wang, Y. He, B. Bramer, and M. Al-Akaidi, "Investigation of biological phantom for 2D and 3D breast EIT images," in *Proceedings of the 13th International Conference on Electrical Bioimpedance and the 8th Conference on Electrical Impedance Tomography (ICEBI '07)*, vol. 17, part 10, pp. 328–331, Graz, Austria, September 2007.

[218] J. Conway, "Electrical impedance tomography for thermal monitoring of hyperthermia treatment: an assessment using in vitro and in vivo measurements," *Clinical Physics and Physiological Measurement A*, vol. 8, no. 4, pp. 141–146, 1987.

[219] T. K. Bera and J. Nagaraju, "A reconfigurable practical phantom for studying the 2 D Electrical Impedance Tomography (EIT) using a FEM based forward solver," in *Proceedings of the 10th International Conference on Biomedical Applications of Electrical Impedance Tomography*, School of Mathematics, The University of Manchester, Manchester, UK, June 2009.

[220] S. Ahn, S. C. Jun, J. K. Seo, J. Lee, E. J. Woo, and D. Holder, "Frequency-difference electrical impedance tomography: phantom imaging experiments," *Journal of Physics*, vol. 224, no. 1, Article ID 012152, 2010.

[221] I. D. Schneider, R. Kleffel, D. Jennings, and A. J. Courtenay, "Design of an electrical impedance tomography phantom using active elements," *Medical and Biological Engineering and Computing*, vol. 38, no. 4, pp. 390–394, 2000.

[222] L.-H. Juang and M.-N. Wu, "Image noise reduction using Wiener filtering with pseudo-inverse," *Measurement*, vol. 43, no. 10, pp. 1649–1655, 2010.

[223] M. Z. Ur Rahman, G. V. S. Karthik, S. Y. Fathima, and A. Lay-Ekuakille, "An efficient cardiac signal enhancement using time-frequency realization of leaky adaptive noise cancelers for remote health monitoring systems," *Measurement*, vol. 46, no. 10, pp. 3815–3835, 2013.

[224] A. Jeanvoine, D. Gnansia, E. Truy, and C. Berger-Vachon, "Source detection: influence of the Doerbecker's noise reduction algorithm; Simulation in the case of binaural cochlear implant coding," *Measurement*, vol. 47, pp. 240–247, 2014.

[225] I. J. Amin, A. J. Taylor, F. Junejo, A. Al-Habaibeh, and R. M. Parkin, "Automated people-counting by using low-resolution infrared and visual cameras," *Measurement*, vol. 41, no. 6, pp. 589–599, 2008.

[226] Y.-H. Wang, J. Qiao, J.-B. Li, P. Fu, S.-C. Chu, and J. F. Roddick, "Sparse representation-based MRI super-resolution reconstruction," *Measurement*, vol. 47, pp. 946–953, 2014.

[227] W. D. Hou and Y. L. Mo, "Increasing image resolution in electrical impedance tomography," *Electronics Letters*, vol. 38, no. 14, pp. 701–702, 2002.

[228] E. Yoshida, H. Yamashita, H. Tashima et al., "Design study of the DOI-PET scanners with the X'tal cubes toward sub-millimeter spatial resolution," *Journal of Medical Imaging and Health Informatics*, vol. 3, pp. 131–134, 2013.

[229] G. Sun, C. R. French, G. R. Martin et al., "Comparison of multifrequency bioelectrical impedance analysis with dual-energy X-ray absorptiometry for assessment of percentage body fat in a large, healthy population," *American Journal of Clinical Nutrition*, vol. 81, no. 1, pp. 74–78, 2005.

[230] J. R. Mager, S. D. Sibley, T. R. Beckman, T. A. Kellogg, and C. P. Earthman, "Multifrequency bioelectrical impedance analysis and bioimpedance spectroscopy for monitoring fluid and body cell mass changes after gastric bypass surgery," *Clinical Nutrition*, vol. 27, no. 6, pp. 832–841, 2008.

[231] S. Gawad, T. Sun, N. G. Green, and H. Morgan, "Impedance spectroscopy using maximum length sequences: application to single cell analysis," *Review of Scientific Instruments*, vol. 78, no. 5, Article ID 054301, 2007.

[232] T. Sun, D. Holmes, S. Gawad, N. G. Green, and H. Morgan, "High speed multi-frequency impedance analysis of single particles in a microfluidic cytometer using maximum length sequences," *Lab on a Chip*, vol. 7, no. 8, pp. 1034–1040, 2007.

[233] T. Sun, S. Gawad, C. Bernabini, N. G. Green, and H. Morgan, "Broadband single cell impedance spectroscopy using maximum length sequences: theoretical analysis and practical considerations," *Measurement Science and Technology*, vol. 18, no. 9, pp. 2859–2868, 2007.

[234] J. M. Porter, I. D. Swain, and P. G. Shakespeare, "Measurement of pulsatile limb and finger blood flow by electrical impedance plethysmography: criteria for the diagnosis of abnormal flow," *Journal of Biomedical Engineering*, vol. 9, no. 4, pp. 367–373, 1987.

[235] J. M. Porter, I. D. Swain, and P. G. Shakespeare, "Measurement of pulsatile limb and finger blood flow by electrical impedance plethysmography: criteria for the diagnosis of abnormal flow," *Journal of Biomedical Engineering*, vol. 9, no. 4, pp. 367–373, 1987.

[236] R. Shankar, S. Y. Shao, and J. G. Webster, "A Fully Automated Multichannel Digital Electrical Impedance Plethysmograph," 2008, http://csi.fau.edu/wp-content/uploads/2013/01/Fully_Automated_Multi_Channel_Plethysmograph.pdf.

[237] R. Shankar, M. Gopinathan, and J. G. Webster, "Digital Signal Processing in Clinical Validation Studies with Impedance Plethysmography," 2008, http://csi.fau.edu/wp-content/uploads/2013/01/Digital_Signal_Processing_Impedance_Plethysmography.pdf.

[238] R. Shankar, M. Martinez, and J. G. Webster, *Software Protocol Techniques for Clinical Validation Studies with Impedance Plethysmography*, 2008.

[239] M. Saritha, K. P. Joseph, and T. M. Abraham, "Automatic interpretation of MRI brain images using probabilistic neural network," *Journal of Medical Imaging and Health Informatics*, vol. 3, pp. 237–241, 2013.

[240] E. Schwartz and L. Shamir, "Correlation between brain MRI and continuous physiological and environmental traits using 2D

global descriptors and multi-order image transforms," *Journal of Medical Imaging and Health Informatics*, vol. 3, pp. 12–16, 2013.

[241] E. A. Zanaty, "An approach based on fusion concepts for improving brain Magnetic Resonance Images (MRIs) segmentation," *Journal of Medical Imaging and Health Informatics*, vol. 3, pp. 30–37, 2013.

[242] Mohanalin, P. K. Kalra, and N. Kumar, "Poisson's equation based image registration: an application for matching 2D mammograms," *Journal of Medical Imaging and Health Informatics*, vol. 4, pp. 49–57, 2014.

[243] T. M. Oliveira, T. K. Brasileiro Sant'Anna, F. M. Mauad, J. Elias Jr., and V. F. Muglia, "Breast imaging: is the sonographic descriptor of orientation valid for magnetic resonance imaging?" *Journal of Magnetic Resonance Imaging*, vol. 36, no. 6, pp. 1383–1388, 2012.

[244] K. K. Lindfors, J. M. Boone, M. S. Newell, and C. J. D'Orsi, "Dedicated breast computed tomography: the optimal cross-sectional imaging solution?" *Radiologic Clinics of North America*, vol. 48, no. 5, pp. 1043–1054, 2010.

[245] H. -K. Wu, H. -S. Tseng, L. -S. Chen et al., "Flow index of 3D breast ultrasound was strongly correlated with axillary lymph node metastasis in the absence of lymphovascular invasion," *Journal of Medical Imaging and Health Informatics*, vol. 4, pp. 66–70, 2014.

[246] J. M. Boone, A. L. C. Kwan, K. Yang, G. W. Burkett, K. K. Lindfors, and T. R. Nelson, "Computed tomography for imaging the breast," *Journal of Mammary Gland Biology and Neoplasia*, vol. 11, no. 2, pp. 103–111, 2006.

[247] E. L. Rosen, W. B. Eubank, and D. A. Mankoff, "FDG PET, PET/CT, and breast cancer imaging," *Radiographics*, vol. 27, supplement 1, pp. S215–S229, 2007.

[248] Y. Zhou, "Ultrasound diagnosis of breast cancer," *Journal of Medical Imaging and Health Informatics*, vol. 3, pp. 157–170, 2013.

[249] D. M. Ikeda, D. R. Baker, and B. L. Daniel, "Magnetic resonance imaging of breast cancer: clinical indications and breast MRI reporting system," *Journal of Magnetic Resonance Imaging*, vol. 12, no. 6, pp. 975–983, 2000.

[250] A. C. Silva, B. G. Morse, A. K. Hara, R. G. Paden, N. Hongo, and W. Pavlicek, "Dual-energy (spectral) CT: applications in abdominal imaging," *Radiographics*, vol. 31, no. 4, pp. 1031–1050, 2011.

[251] W. A. See and L. Hoxie, "Chest staging in testis cancer patients: imaging modality selection based upon risk assessment as determined by abdominal computerized tomography scan results," *Journal of Urology*, vol. 150, no. 3, pp. 874–878, 1993.

[252] K. B. Kim, H. J. Park, S. Kim, and S. J. Lee, "Extraction and analysis of muscle areas from abdominal ultrasonographic images," *Journal of Medical Imaging and Health Informatics*, vol. 4, pp. 8–13, 2014.

[253] M. Gupta, D. L. Schriger, J. R. Hiatt et al., "Selective use of computed tomography compared with routine whole body imaging in patients with blunt trauma," *Annals of Emergency Medicine*, vol. 58, no. 5, pp. 407–e15, 2011.

[254] G. P. Schmidt, H. Kramer, M. F. Reiser, and C. Glaser, "Whole-body magnetic resonance imaging and positron emission tomography-computed tomography in oncology," *Topics in Magnetic Resonance Imaging*, vol. 18, no. 3, pp. 193–202, 2007.

[255] S. J. Eustace and E. Nelson, "Whole body magnetic resonance imaging," *British Medical Journal*, vol. 328, no. 7453, pp. 1387–1388, 2004.

[256] K. U. Juergens, M. L. Oei, M. Weckesser et al., "Whole-body imaging of oncologic patients using 16-channel PET-CT: evaluation of an IV contrast enhanced MDCT protocol," *NuklearMedizin*, vol. 47, no. 1, pp. 30–36, 2008.